LBL – PUB-5390

U10.0 Undulator Conceptual Design Report

ALS Insertion Device Group

June 1994

Table of Contents

Summary

The U10.0 Undulator described here is a 43 period, 10 cm period, 4.5 meter long insertion device. Designed for the Advanced Light Source (ALS) storage ring at the Lawrence Berkeley Laboratory. This insertion device will provide high brightness, quasi-monochromatic radiation in the 5–950 eV energy range.

This conceptual design report includes sections on: parameter development, spectral performance, and accelerator requirements, physics specifications and the detailed conceptual design of the magnetic structure, the support/drive systems, the insertion device control system, the vacuum system, and installation for the U10.0 Undulator.

1.0 Scope

The purpose of this conceptual design report is to assemble in a single document the preliminary design of the *U10.0 Undulator. This report describes the establishment of the parameters,* the performance, the specifications, and the proposed design. Adoption of this conceptual design report will provide a baseline design from which a detailed design of the U10.0 Undulator can follow.

Specifically, the sections of this conceptual design report include:

Section	Description
2.0	PARAMETER DEFINITION AND REVIEW PROCESSES—How the U10.0 parameters were established, how they can be changed, and the planned review process to insure an acceptable design.
3.0	INSERTION DEVICE PERFORMANCE—U10.0 Spectral performance and accelerator requirements.
4.0	INSERTION DEVICE SPECIFICATIONS—U10.0 Physics and the magnetic measurement specifications.
5.0	INSERTION DEVICE CONCEPTUAL DESIGN—Detailed conceptual design descriptions of the subsystems of the U10.0 undulator. The subsystems include:

Section	Subsystem
5.1	Design Philosophy
5.2	Design Parameters
5.3	Magnetic Structure
5.4	Insertion Device Magnetic Measurement Facility
5.5	Support/Drive System
5.6	Insertion Device Control System
5.7	Vacuum System
5.8	Installation

The cost estimate and the associated fabrication schedules for the *U10.0 Undulator* are found elsewhere.[1]

2.0 PARAMETER DEFINITION & REVIEW PROCESSES

The parameters for the insertion device for the ALS are determined from a broad range of requirements that have been evolving since the Advanced Light Source was first proposed in 1982. However, there are three major areas that combine to establish the ID parameters. These are:

- Spectral requirements, as proposed by the potential users of the ALS,
- Accelerator design, as developed by the ALS Accelerator Physics and Engineering Groups,
- Performance and tolerance limits for the mechanical, magnetic, and eiectrical components, as developed by the ALS Experimental Systems and Engineering Groups.

2.1 Parameter Changes

Following the conceptual design review, this document will be updated and will establish the baseline U10.0 Undulator design parameters. To change the parameters after this point in the process will require a formal review of the proposed changes along with an assessment of the impact the changes will have on device performance, cost, and schedules. Parameter changes are initiated by submitting a proposed change on an ALS Parameter List/Scope Change Authorization Form, submitting it to the Project Office. To be approved, the proposed change must be reviewed by the following three groups: Accelerator Physics, Experimental Systems, and Engineering.

2.2 Review Process

Adoption of this conceptual design report establishes a baseline conceptual design for the U10.0 Undulator. The follow on to this conceptual design is the detailed design of the various subsystems and the respective final design reviews of these subsystems prior to commencing fabrication.

For the U10.0 Undulator, the subsystem designs are very similar to those of the already completed U8.0 Undulator so final design reviews are not planned.[2]

3.0 INSERTION DEVICE PERFORMANCE

3.1 Spectral Requirements

The U10.0 Undulator will be the fourth of a family of insertion devices to be built and installed on the ALS. This 43 period, 10 cm period, 4.5 meter long device is designed to operate in a range of energies from 5 eV to 950 eV, as shown in Fig. 1. To cover this range requires two conditions: 1) operating at 0.98 T B_{eff} at minimum gap to reach the lowest energy, and 2) the ability to produce a high brightness in the 1st, 3rd, and 5th harmonics. The former can be accomplished by designing a robust magnetic structure, while achieving the latter depends on understanding the characteristics of the accelerator and establishing appropriate error tolerances for the U10.0 design.

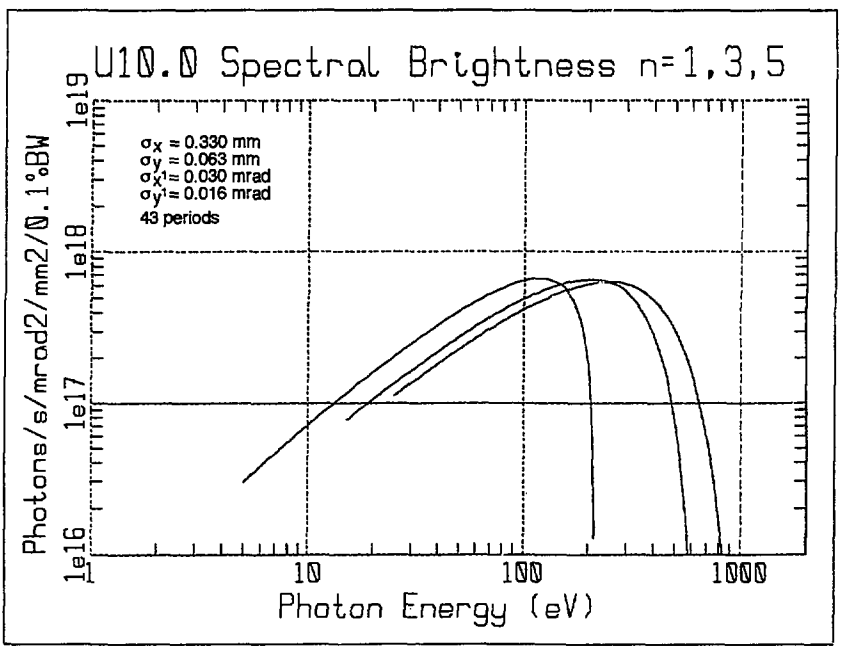

FIG. 1. U10.0 Undulator brightness over the usable photon energy range.

The most stringent requirements on the U10.0 Undulator design come from the goal of a high brightness 5th harmonic and storage ring limits on integrated quadrupoles. The intensity of the light in a spectral peak from an insertion device is limited by the characteristics of the electron beam and the field errors in the device itself. Only the error fields perpendicular to the average electron beam axis are considered; field errors parallel to the electron beam axis cause a small beam displacement, but no steering or other significant detrimental effects. These field errors can be considered in two separate groups: random and systematic. The random errors cause the brightness of a spectral peak to be reduced. The reduction in spectral performance associated with a random field error causes light to be produced over a broad range of frequencies outside the peak itself. The effect of a given set of magnetic field errors on spectral output can be calculated, however, error limits must be established before a device is constructed.

The relationship between the reduction in spectral brightness and the random field errors is shown in Fig. 2.[3] This relationship is the result of an analytic calculation for a statistical ensemble average. This does not necessarily apply to any single device. In the figure, N is the number of undulator periods, σ is the *rms* field error, n is the harmonic number, and K is the deflection parameter. Functions G_Δ and F_Δ describe intensity loss and peak position shift for small and large orbit walks, respectively. If we allow a 30% reduction in the peak intensity then the allowable random field error is 0.43% for U10.0, which becomes the requirement. This limit is similar to that observed in other devices. The BL X Wiggler at SSRL and the TOK at NSLS both have random magnetic field errors that are similar to this value.

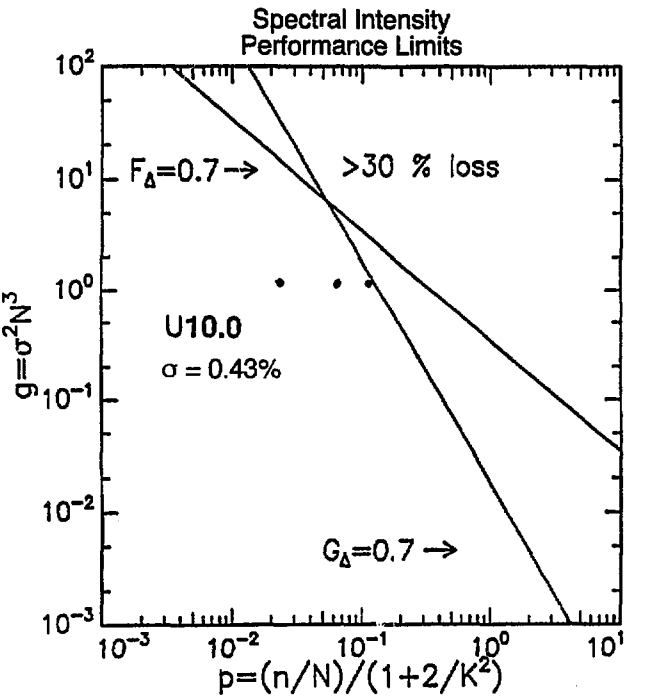

FIG. 2. Spectral brightness limits.

Systematic errors in the magnetic field produce a very different type of effect on spectral performance. Variations in both field B and in period λ produce a chirp in the frequency of the light produced. The result is a broadening of the peak, while the total power in the peak remains approximately constant.

The characteristic linewidth for a perfect insertion device is determined by the machine characteristics, the number of periods, and the spectral harmonic number. Here, we restrict the systematic field errors to a level where their contribution to spectral width is equal to the linewidth of the 5th harmonic in a perfect device.

Several parameters for the insertion device that are determined by user requirements are summarized in Table I. These include: 1) the rate at which the frequency of the emitted light can be changed—which is related to the

rate of variation in K, B, and gap, and 2) the minimum frequency shift that can be made—which is related to the minimum increment in gap that is possible. These two parameters are controlled by the limits associated with the requirement to produce a usable 5th harmonic. Good spectral performance requires that the steering error be small throughout the insertion device. Since no significant systematic dipole fields were observed in the periodic sections of the other ALS devices, we have eliminated the U5.0 and U8.0 requirements of having the capability of producing local fields of the order of 5 G to provide horizontal steering within the device.

The variation in K along the insertion device will produce a "chirp" in the spectrum, thus, broadening and reducing the height of the peak. Based on a goal of a usable 5th harmonic, we allow the variation of K along the device to broaden this harmonic by, at most, an amount equal to the characteristic width of the line that would exist if the insertion device were perfect and if the machine were operating in its normal multibunch mode. Thus, the maximum allowable increase in linewidth over the ideal case is 0.5%.

TABLE I. Requirement for the ALS insertion device.

Parameter	Value
Useable harmonics	1st, 3rd, & 5th
Minimum increment of photon energy	< 1/10 of 5th bandwidth ~ 0.05%
Minimum incremental gap motion	2.8 μm
Minimum time to go from minimum to maximum gap (slew)	1 minute
Maximum controlled photon energy scan rate	1 bandwidth/second

3.2 Accelerator Requirements

The beam in the accelerator is affected in two general ways by the magnetic fields in the insertion devices. The first is associated with the fields expected in a perfect device and the second with the possible error fields. In addition, the electrons will interact with any ions trapped in the combined fields of the electron beam and the insertion devices. Each of these items must be addressed in the process of insertion device design.

In a perfect device, the periodic fields produce focusing in the vertical plane of the storage ring. For electrons in the core of the beam this focusing requires minor adjustments of the strengths of the storage ring quadrupoles. However, this focusing causes a break in the natural periodicity of the magnet lattice, which leads to a reduction of the dynamic aperture. Further, the higher spatial harmonics intrinsic to the perfect device contribute to perturbing forces that limit the momentum acceptance of the storage ring. Both these effects lead to a reduction of beam lifetime.

These phenomena have been studied by using tracking codes by the Accelerator Systems Group. They concluded that the effects of undulators (operating at their maximum fields) on the dynamic aperture of an otherwise perfect machine, were substantial. However, the machine acceptance, which determines the gas scattering lifetime, was limited by the vacuum chamber gap in the insertion device itself, not by the reduction in dynamic

aperture. When other machine imperfections were considered, an unexpected phenomenon was observed, causing a reduction in the Touschek lifetime. This effect is still under investigation. However, the results to date indicate that the resulting beam lifetime, including the effects of both insertion devices and the machine imperfections, will be acceptable.

The fact that the insertion devices have an effect on the machine must be balanced against other effects inherent in a real machine. For example, if the field errors in the ring accelerator magnets are considered alone, there is a significant decrease in the dynamic aperture. The effects of both have been calculated and the expectation at present is that insertion devices meeting the proposed specifications will not cause noticeable degradation of the dynamic aperture of the ALS beyond that produced by other errors.

Error fields are introduced by construction tolerances, as well as by the intrinsic fields of the insertion devices. The main problem with these field components, as far as the storage ring is concerned, is that they change as the undulator field changes. Correction elements that compensate for the linear terms are included in the machine. However, to compensate for the effects of each scanning device simultaneously will require action by the control system. Therefore, specifications are developed for the error fields that will have a minimal effect on the storage ring, possibly without the necessity for compensation.

The first and second integrals of the principal field, B_y, should be zero for all values of the gap. Non-zero integrals will lead to an electron beam displacement in the insertion device and a net kick. One of the most significant effects of vertical error field will be horizontal distortions of the electron orbit at other places around the ring. These distortions can be significantly larger than the displacements in the device and can have a significant effect on the performance of other insertion devices and their experimental beam lines. The limit set on the vertical field integral is 100 G cm.

There will be some horizontal magnetic fields perpendicular to the beam in the device due to various errors. These fields are not easily calculable, but their limit can be set based on steering requirements at a somewhat higher level, 500 G cm. They will be corrected by the ALS steering magnets.

The above values are relatively small, but within the range of measurements that have been made for the other devices built and measured by LBL.

In addition to net dipole fields in the devices, there is the need to assure that off-axis particles are not focused by integrated fields in the device, and that the beam will not be steered incorrectly if it does not pass exactly down the center. These requirements establish the limits on the allowable quadrupole, skew quadrupole, and sextupole. These are presently set at 100 G cm/cm, 100 G cm/cm, and 100 G cm/cm^2, respectively. Furthermore, so as not to degrade beam lifetime, field integrals must remain relatively uniform over the entire ±1 cm vertical by ±3 cm horizontal "good field region", which extends outside the convergence radius for expansion in multipoles. Integrated fields and gradients everywhere in this region should not exceed 100 G cm and 100 G cm/cm, respectively.

There are questions associated with the commissioning of the machine that affect the insertion devices. To achieve a high magnetic field in the devices, it is necessary to have the gap as small as possible. For both comissioning and normal operation, we have chosen 2.35 cm as the minimum gap, which corresponds to a vacuum chamber aperture of 1.9 cm.

The machine requirements placed on the insertion device are summarized in Table II, including the vacuum requirement of 10^{-9} Torr, which is typical of the entire machine.

TABLE II. Requirements on the ALS insertion devices.

Parameter	Limit
$\int B_y \, dl$	100 G cm
$\iint B_y \, ds \, dl$	100 G cm^2
$\int B_x \, d\,l$	500 G cm
Integrated quadrupole	100 G cm/cm
Integrated skew quadrupole	100 G cm/cm
Integrated sextupole	100 G cm/cm^2
Required vacuum	10^{-9} Torr

4.0 INSERTION DEVICE SPECIFICATIONS

4.1 Magnetic Structure

The U10.0 Undulator will incorporate the hybrid magnetic configuration consisting of Nd-Fe-B magnetic blocks and vanadium permendur poles. The hybrid is chosen because of several advantages over the pure current sheet equivalent material (CSEM) design.

- The field is dominated by the characteristics of the poles, which can be made uniform both in size and magnetic performance.
- The errors in magnetic moments of the blocks can be averaged by sorting the blocks for the poles.
- Errors in the total magnetic moment of all the blocks on a pole have little effect on the electron beam, or the spectrum, because they contribute equally to adjacent poles and produce no electron beam steering.
- The peak field at each pole can be tuned by a small amount.
- A higher peak field is achievable at small gap/period ratios.

4.1.1 Magnetic Structure Requirements

The engineering tolerances for construction of the U10.0 Undulator for the ALS are based on the design performance of the device as installed. Two types of errors affect the performance limits in different ways. In the first, the set of random errors associated with the characteristics and placement of individual components of the insertion device cause a reduction in spectral brightness. In the second, the set of systematic variations in gap that broaden the spectral peaks—the allowable systematic errors—are related to the quality of the ALS electron beam.

The effects of the random errors are determined by a set of calculations that are based on the hybrid CSEM insertion device theory developed by K. Halbach.[4] Possible errors, shown in Fig. 3, include vertical motion of a pole, variations in pole thickness, misorientation of the CSEM's easy-axis near the electron beam, and different spacings between the two poles and the CSEM block in a half period. In this section, we generate the values for the engineering tolerances for U10.0 from the error calculations.[5,6] The magnitude of each error, mentioned above, which will produce a 0.1% variation (σ) in the integrated flux crossing the midplane, per single half period, is given in Table III.

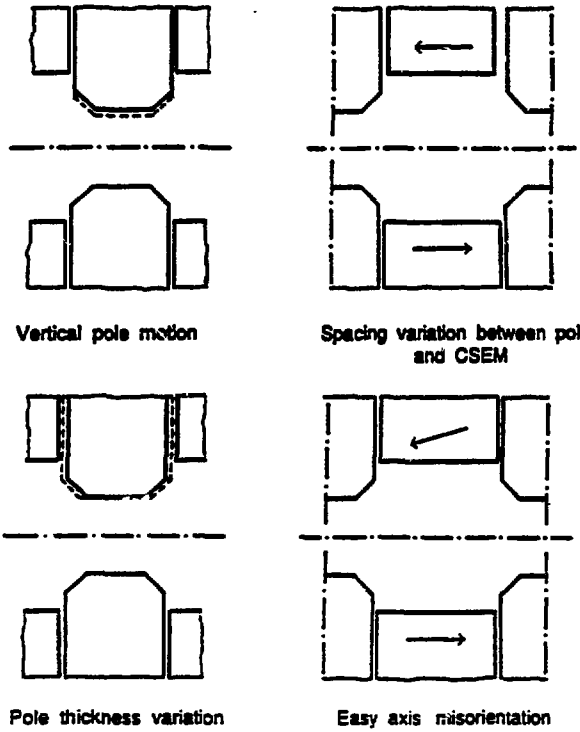

FIG. 3. Hybrid magnetic structure errors.

TABLE III. Summary of individual errors that produce a 0.1% variation (σ) in the integrated flux across the midplane for the U10.0 magnetic design gap of 2.36 cm.

Error Type	U10 Value
Vertical pole motion	50 μm
Pole thickness	120 μm
Easy-axis orientation (closest block to beam)	0.6 degrees
Spacing variation between poles and CSEM	40 μm

One important goal of the design of the U10.0 is to limit the reduction in the spectral peaks associated with random errors in the magnetic field to 30%. This decrease in performance would be associated with the characteristics of an ensemble of insertion devices with random magnetic field errors of about 0.43%. Using 0.43% as the allowable random field error, and assuming that all errors add in quadrature, each of the errors in Table III can be assigned an error tolerance that is a fraction of this value. Further, the relative contributions can be adjusted depending on design criteria.

It is necessary, for the purpose of building a device, to discuss the limits in the form of mechanical tolerances rather than errors. The relation between an error σ and a mechanical tolerance can be determined by assuming a uniform distribution of any parameter within the tolerance *t* and requiring that the mean square variation be the equivalent to that of a Gaussian. The conclusion is that a tolerance *t* should be about 1.73 times the equivalent error σ based on a Gaussian distribution.

Of the several errors to be considered, there are two—the CSEM centering error and the pole width error—that are easy to control. These are addressed first, followed by the pole position error, which is determined by machine requirements, and the remaining error allowance is used to determine the maximum allowable easy-axis orientation error in the Nd-Fe-B blocks.

The variation in the spacing between the CSEM and each side of the poles is determined by the tolerance buildup of poles, CSEM, and holder. It is possible to ascribe a maintainable tolerance of 100 mm to this difference, corresponding to a σ of 60 μm, or 0.15%, which will be combined with the other errors.

The pole thickness can easily be controlled to 50 μm, which leads to a σ of 30 μm or 0.03%.

The error tolerance on vertical pole position is determined by two considerations. The first is the limit on quadrupole field in the insertion device. The other is the random field error at the midplane.

Pole tilt can introduce quadrupole fields. The effect of pole tilt on the random field error is small, but the maximum allowable quadrupole field limits the relative tilt of a pair of poles to 0.32 mrad, or 26 μm over the width of the 8 cm pole. Using this same value as the tolerance for the gap variation, the random error contribution will be 0.03%.

There can be errors in pole width. Using an approach similar to the one used with pole thickness errors, the pole width tolerance is 100 microns, which contributes little to the total error.

The final major error is associated with misorientation of the easy axis. Having determined the other errors, the vertical easy-axis orientation error could be allowed to reach 3.0 degrees, thus, contributing 0.29% to the error budget. Nonetheless, those blocks centered just above or below the axis, will be those with the smallest easy-axis orientation errors (<<3 degrees).

The error types, assigned tolerances, and magnetic field error contributions (σ) for the U10.0 Undulator are summarized in Table IV.

Table IV. Summary of magnetic tolerances for the U10.0 Undulator.

Error Type	Total Tolerance	Error (%)
Spacing CSEM to pole	100 μm	0.15
Pole thickness	50 μm	0.03
Vertical pole motion (gap)	26μm	0.03
Pole width	100 μm	0.04
Easy-axis orientation	± 3.0 degree	0.29
	Total:	**0.33**

The goal of achieving high brightness beams requires that the insertion device be as long as possible, 4.5 m, and have as many full periods as possible. However, it must also meet entrance and exit pole requirements. A total of two periods are sacrificed to provide appropriate steering and displacement over a range of gaps.

Spectral performance of the first three ALS undulators (two U5.0s and a U8.0) easily meets specifications. Integrated multipole fields initially did not meet accelerator requirements; superposition of non-random, easy-axis orientation errors of blocks positioned transversely off-center was a major cause. Needed correction was provided by sets of multiple trim magnets situated at both upstream and downstream undulator ends. Both normal and skew integrated fields over the entire ±1 cm by ±3 cm 'good field region' were corrected to within tightened specifications, which included gradient limits outside the multipole convergence radius. Additionally, these trim magnet arrays provided for correction of the linear component of integrated field gradients for particles with trajectories not parallel to the nominal beam axis. U10.0 permanent magnet block sorting will reduce the above mentioned integrated field error source. Still, U10.0 will make use of convenient multiple trim magnet arrays at undulator ends to further reduce these integrated fields.

U10.0 has a larger wiggle amplitude (50μm) than does U5.0 (11.4 μm), and thus through the ID, a larger horizontal offset from the nominal (unperturbed) beam axis were the ends to be configured with pole scalar potentials of 0, +1/2, -1, +1, etc. For scanning experiments, it is desirable to have horizontal beam position stable while changing the gap; thus U10.0 is designed with a 0, +1/4, -3/4, +1, -1, etc. scalar potential end configuration, making average beam displacement through the insertion device zero with respect to the nominal beam axis. This excitation is made as gap-independent as possible.

Unlike the ALS U5.0 and U8.0 devices, the U10.0 will feature an even number of poles. This is to cancel the integrated sextupole-like component that comes from the ends of the device, and which affects particle trajectories parallel to the nominal beam axis.

The final set of parameters for the insertion device conceptual design are given in Section 5.2, Table V.

4.1.2 Requirements for CSEM Blocks

Two types of blocks have been considered for the U10.0 insertion device, samarium cobalt Sm-Co and neodymium iron boron Nd-Fe-B. The advantage of Sm-Co is its high resistance to radiation, whereas Nd-Fe-B is a higher performance material. Because the U10.0 can be expected to operate on the ALS for as long as 20 years, it was necessary to assess the possible effects of radiation over this period of time on these materials. A complete evaluation of this topic for the ALS insertion devices is given elsewhere.[7] The conclusions are summarized here.

The expected ionizing radiation in each ALS insertion device, based on the assumption that half the beam is lost during each fill in 5 of the insertion devices and that there are 1,000 fills of the ALS per year, is only 3×10^6 rads. The limited data on Nd-Fe-B suggest that this level of radiation is below the level where there is a detectable effect on the material performance. The effect expected from neutron radiation during the 20 year life of a device is even less.

During this study, there was an evaluation of the effect of shielding of the insertion device by the vacuum chamber. Both aluminum and stainless steel have been used successfully for this type of vacuum chamber. The aluminum chamber is less expensive and has better thermal conductivity. However, because the stainless steel has a higher density and a higher atomic number Z, it was thought that it might provide better shielding. A study using the EGS4 code was carried out at SLAC and the results show that there is little difference in this regard between aluminum and stainless steel.[8]

The CSEM blocks that are used for insertion devices have typically been characterized by their three magnetic moments. Because of the tight requirement on the allowable field errors in U10.0, measurements of just these three moments may not be adequate. The field errors in devices, such as the TOK at BNL-NSLS and the BL X Wiggler at SSRL, show large field variations in the regions between the poles, which indicate that the effects of

local field perturbations produced by the magnetic materials closest to the electron beam can have a significant contribution to the error fields.

This suggests two approaches. First, the block size should be chosen so that there is a single block directly above the electron beam, i.e., there will be an odd number of blocks across the pole. We have chosen three blocks for the U10.0 configuration. Second, the usual sorting algorithm for the block material, which is typically based primarily on the principal moment, should be expanded to include the easy-axis orientation errors.

Studies of the relationship between the surface fields and the easy-axis orientation errors in some spare blocks from the BL X Wiggler showed little correlation between the local surface field and the, presumably equivalent, easy-axis moment components produced by the easy axis. However, due to the cost of measuring blocks and the availability of the multiple trim magnets, the surface fields of the blocks in the U10.0 will not be measured.

The Nd-Fe-B material used in the blocks must be of high quality. A coercive force, H_c, greater than 10.6 kOe, is specified. The magnetization must also be linear, to 120% of H_c (third quadrant) at a temperature of 50 degree C after thermal stabilization.

The block dimensions are determined by a complete magnetic analysis of the structure and are developed in Section 5.3.1. However, dimensional tolerances for the blocks are determined by: assembly procedures, overall tolerances of the set of blocks as they are bonded into the pole assembly, and the final assembly of the device. These considerations allow a dimensional tolerance of 60 μm for the block thickness.

The variation of the dipole moment of the individual blocks is determined by an assigned 0.1% standard deviation allowed in the total magnetization on the poles.

The Nd-Fe-B blocks must also be supplied with appropriate surface preparation for good adhesion in the pole/keeper assembly, and to avoid oxidation over the expected life of the device.

4.1.3 Backing Beam Requirements

The spectral width of the output of an insertion device is determined by the following factors:

- The intrinsic linewidth;
- The momentum spread of the electron beam;
- The angular divergence of the electron beam;
- The systematic variation of K along the insertion device.

The first of these is determined by the insertion device design. The next two depend on the machine and its operating conditions. The last item is determined, to first order, by the structural rigidity of the device and the temperature gradients in the structure, which lead to gap variations. In this section, we describe the effects of each of these items on spectral linewidth, discuss the various ALS operating conditions and use these as inputs to establish a limit on the systematic gap variation for U10.0.

Intrinsic Linewidth

The insertion device U10.0 will be 4.5 meters long and will have nominally 43 periods. One performance goal for U10.0 is to have a usable 5th harmonic. Thus, the intrinsic linewidth, in terms of the σ of the 5th spectral harmonic of a 43 period undulator, is given by:

$$\sigma_\lambda \frac{1}{2.35}\text{FWHM} = \frac{1}{2.35nN} = 0.200\%$$

where the factor of 2.35 between FWHM and σ_λ has been included, n=5 is the harmonic number and N=43 is the number of periods. This is the width of the line produced by a single electron passing through the device.

Momentum Spread

Not all the electrons in the ALS have exactly the same momentum. The momentum spread of the beam depends on the operating conditions. The values of $\Delta p/p$ or σ_p that can be expected are:

$$\Delta p/p = \begin{cases} 0.08\% \text{ multibunch mode} \\ 0.16\% \text{ multibunch mode (low density)} \\ 0.13\% \text{ single bunch mode} \end{cases}$$

The most likely operating condition is the multibunch mode, with a $\Delta p/p$ of 0.08%, though one might expect on occasion to operate at the lowest possible momentum spread of 0.06% to limit spectral broadening.

For the multibunch mode $\sigma_\lambda = 2\sigma_p = 0.16\%$.

Angular Divergence

The electron beam angular divergence also affects the linewidth. Electrons that are not exactly on-axis produce light on-axis that is slightly lower in energy than that from on-axis electrons, which gives a skewed distribution in the spectrum rather than a simple Gaussian. This can be seen from the following relation. For small angles, $\theta\gamma << 1$

$$\frac{\Delta\lambda}{\lambda_o} = \frac{\gamma^2\theta^2}{1+\frac{K^2}{2}},$$

where λ_o is the on-axis wavelength.

Given the distribution of electrons in θ, $v(\theta)$, we can calculate the distribution in λ,

$$n(\theta) \propto e^{-\left(\frac{\theta^2}{2\sigma_\theta^2}\right)}$$

The distribution in λ can be shown to be a one sided decaying exponential. The question is how to extract a reasonable value of $\sigma_{\lambda\theta}$ that can be compared and combined with the variations of the other parameters. The approximation used here is to first find the value of $\Delta\lambda$ when $n(\Delta\lambda)$, and also $n(\theta)$, is 0.5 and assign $1/\sqrt{2}$ of this value to $\sigma_{\lambda\theta}$.

Thus:

$$n(\Delta\lambda) = 0.5 \Rightarrow \frac{\Delta\lambda}{\lambda} \cong \frac{2(\gamma\sigma_\theta)^2}{1+\frac{K^2}{2}} \ln \tfrac{1}{2}$$

$$\sigma_{\lambda\theta} = \frac{0.693(\gamma\sigma_\theta)^2}{1+K^2/2}\frac{2}{\sqrt{2}}$$

This expression must be evaluated for two operating conditions. The first is the specified beam emittance of 10 *nm* radians and the second is the intrinsic emittance of 4 nm radians that might eventually be achieved. These lead to horizontal divergences of 30 and 20 microradians, respectively. (The ratio between *x* and *y* emittances is about 10, so we need only address the *x* emittance here.)

Since the value of $\sigma_{\lambda\theta}$ is affected by K as well as the beam divergence, there is a range of conditions that must be considered. We use two extreme K values, 0 and 10, and the two values described above for the divergence. The standard deviations $\sigma_{\lambda\theta}$ for the two extreme cases are 0.8% and 0.007%. However, as a reference point for further calculations set K = 5 and $\sigma_\theta = 3 \times 10^{-5}$, which gives a $\sigma_{\lambda\theta}$ of 0.03%.

Combining the three effects: intrinsic linewidth, beam momentum spread and beam divergence, there are several possible limits for the effective spectral linewidth $\sigma_{\lambda tot}$ produced by an insertion device with no systematic gap variation. These range from 0.26% to 0.83%, with the reference or performance value $\sigma_{\lambda tot}$ of 0.26%, as given by:

$$\sigma_{\lambda tot}^2 = \sigma_{\lambda i}^2 + \sigma_{\lambda p}^2 + \sigma_{\lambda\theta}^2$$

Gap Variation

Finally, we limit the allowable spectral broadening due to a systematic gap, or K variation, to this inherent standard deviation determined by the storage ring characteristics and the number of periods. The allowable variation in K can be determined by the relation

$$\frac{\Delta K}{K} = \frac{\left(1+\frac{K^2}{2}\right)}{K^2}\frac{\Delta\lambda}{\lambda} = \left(\frac{1}{K^2}+\frac{1}{2}\right)\frac{\Delta\lambda}{\lambda}$$

which, in the limit of large K, becomes

$$\Delta K/K = \frac{1}{2}\frac{\Delta\lambda}{\lambda} \text{ or } \sigma_K = \frac{1}{2}0.26\% = 0.13\%$$

The standard deviation σ_K must be converted into a tolerance, i.e., to the maximum and minimum values of K possible. The factor 1.73 is used for the conversion and noting that the value of K can range both above and below the mean value, the variation in K can be ±0.22%.

This can now be converted into a gap variation by using the following relationship between gap and K:

$$B_o(g) \equiv b_1 e^{\frac{-\pi g}{\lambda_u}}$$

and since $dB/B = dK/K$, for constant λ_u

$$\frac{dK}{K} = \frac{-\pi}{\lambda_u}dg$$

$$\frac{dg}{g} = \frac{-\lambda}{\pi_g}\frac{dK}{K}$$

This gives an allowable gap variation of 140 mm which is most important at minimum gap where the magnetic forces are largest. Thus, it imposes a structural requirement on the backing beam.

4.1.4 End Rotors

Field correction capability will be built into the last two poles at each end of the insertion device. The purpose of these corrections is to provide correct entry and exit of the electron beam and to allow for a correction of some dipole field error. New designs for the end correction have been developed that may allow a single setting for all gaps. Nevertheless, some correction is assumed to be necessary in the end field tuning and there may be the need for gap dependent adjustment. The tuning limit is set here to be equal to 1500 G cm, which corresponds to about 10% of the midplane flux in a single quarter period.

4.1.5 Axial Temperature Gradient

There is an additional limit on the structure associated with the variation in K caused by a temperature gradient axially along the insertion device. Since the allowable variation in K from this effect must be small compared to the variation calculated in Section 4.1.3, and the variation of H in Nd-Fe-B is about 0.12% x per degree C, the axial temperature gradient limit is 2 degrees C for both the operation of the device in the machine and for the magnetic measurements.

4.2 Magnetic Measurement Requirements

Several types of magnetic measurements will be made on the ALS insertion devices and their components. There are two major areas of magnetic measurements that are to be performed: 1) determining the magnetic characteristics of the Nd-Fe-B blocks, and 2) mapping the fields of the entire device.

The requirements for each of these will be discussed in detail below.

4.2.1 Block Measurements

The principal dipole moment of each Nb-Fe-B block that will be used in the insertion device must be measured to an accuracy that will allow subsequent sorting into groups of six blocks to produce a standard deviation of 0.1%, or less for the total moment on a single pole. The blocks proposed for the U10.0 Undulator will have a volume of 71.4 cm^3 and a magnetic moment of about 7.6 x 10^{-5} Wb-m.

The rms allowed variation in the energization of the poles is 0.1%. If this is conservatively ascribed to, the rms deviation for the six blocks together, then the error in determining the quantity must be less, say, half or 0.05%. This leads to an allowable error in the measurement of the moment of each block given by:

$$\frac{\Delta M}{M} = \frac{1}{2}(0.10\%)\sqrt{6} = 0.12\%$$

Two factors can contribute to this error. The first is the measuring system itself, and the second is the temperature at which the block is measured. Moment measurements are considerably more accurate than 0.05% so they will contribute little to this error. However, the temperature coefficient of Nb-Fe-B, 0.12% per degree C, suggests it will be necessary to measure the temperature accurately and control it to better than 1 degree C and correct the measured moments for temperature.

The fields seen by the electron beam are affected by easy-axis orientation of the blocks nearest to the beam. Some Nd-Fe-B blocks left over from the BL X Wiggler were measured to correlate block surface fields, measured with the device shown in Fig. 4, with the moments of the blocks in directions perpendicular to the easy axis. There was little correlation, as shown in Fig. 5, and the surface fields varied considerably across the face of individual blocks. This was in part due to the fact that the blocks, as received, were apparently made up of two blocks.

Thus, we have the capability to perform block surface field measurements if needed. Integrated surface field errors are commensurate with the angle error and must be less than 150 G cm.[9] The measurement accuracy required is 20 G cm.

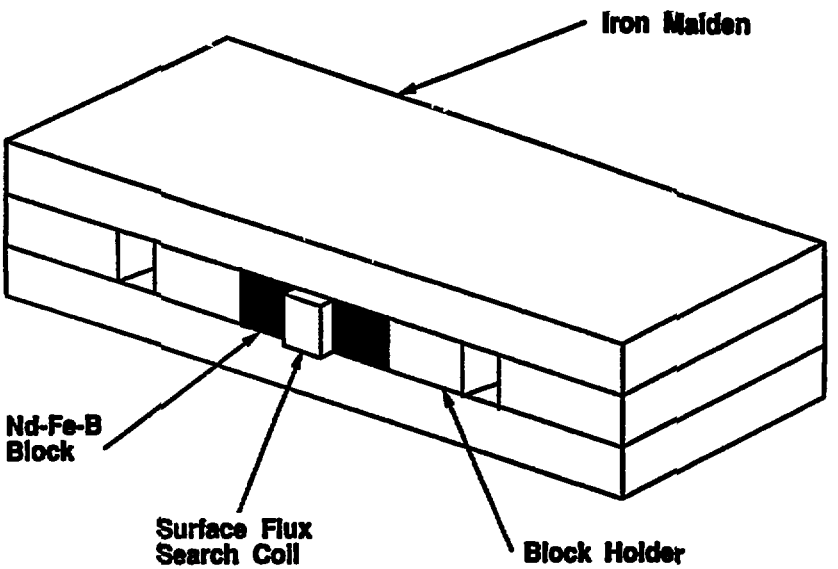

FIG. 4. "Iron Maiden" used for surface magnetic field measurements.

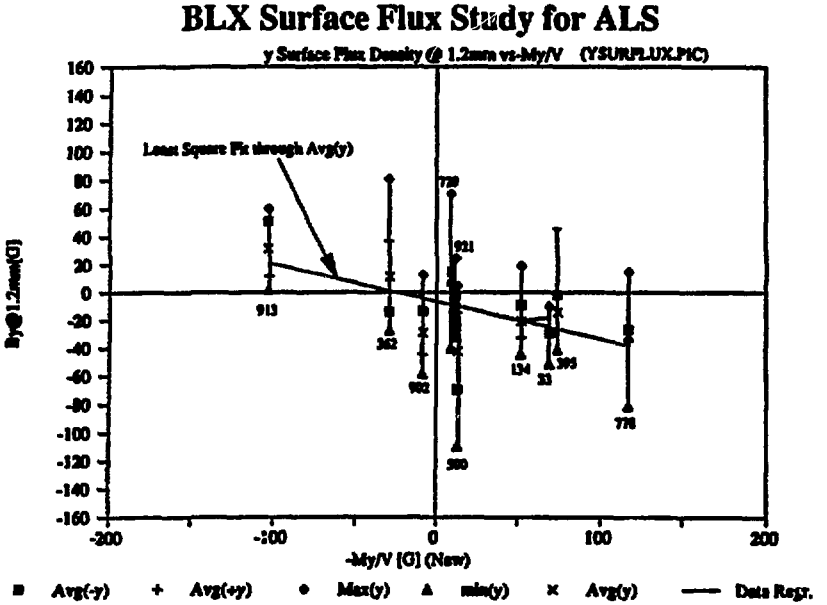

FIG. 5. Surface field versus dipole moment comparison using BLX Wiggler blocks.

4.2.2 Requirements For Measurements of the Full Insertion Devices

The requirements for the magnetic measurement of the full insertion device are based on the two requirements discussed in Section 3.0. Namely, the field quality must be adequate to produce light of the required quality and intensity, and the insertion device must not have an adverse affect on the electron beam in the accelerator. These have been translated into allowable field errors that determine the requirements for the magnetic measurements.

To determine the spectral performance of the U10.0 will require a knowledge of the local fields to <1 G. The limit on the magnetic field integrated along the path of the electrons, both to avoid beam deflection and to assure good spectral output, is 100 G cm. This also requires measurement of the local fields to 1 G or better. This type of measurement accuracy has been achieved by Hall probes with their output integrated later, off-line, or with coils that extend axially for one or more periods. The detailed numerical evaluation of these measurements on all ALS insertion devices must be done while the device is in the measurement facility to allow for adjustment of the end correctors. This places a requirement on the number crunching capability of the computer and workstation needed for the facility.

The ability to measure the fields accurately in an insertion device places tight tolerances on the accuracy with which the measuring probes are positioned. The strong gradients in the axial direction of the principal field, B_y, place the most stringent requirement on positioning and on the position monitoring system. The maximum axial variation of the field is about 0.6 G per μm and the average gradient is about 0.4 G per μm. Typically, axial positioning tolerances of 2.5 μm have been achieved on earlier measurements and are similar to those required here. They are also about the limit expected with laser interferometers over 5 meters.

The requirements for the measurements of the full insertion device are summarized in Table V below and some of the possible scans that will be made are listed in Table VI.

TABLE V. Magnetic Measurement Requirements for the Full Insertion Device.

Parameter	Value
Field measurement	± 2.5 Tesla
Field accuracy	± 1 G
Positioning accuracy *z*	2.5 μm
Positioning accuracy *y*	25 μm
Positioning accuracy *x*	25 μm
Scan capability *z*	-3m → +3m
Scan capability *y*	from 0.3 cm above the lower pole to 0.3 cm below the upper pole
Scan capability *x*	±4.0 cm
Step size *x, y, z*	<1 mm—adjustable
Temperature	±1 degree C
$\int B_y dl$	100 G cm
$\int B_x dl$	100 G cm

TABLE VI. Magnetic Field Scans Required for ALS Insertion Devices.

1. Longitudinal scans of B_y, at ~ 2 mm increments in z, x = 0, y = 0, -3 m < z < +3 m.

2. Combined longitudinal and x-transverse scans of B_y, Δz ~ 2 mm, Δx ~ 5 mm, y = 0, -3 cm < x < 3 cm, -3 m < z < 3 m.

3. Combined longitudinal and *x* & *y* transverse scans of B_y, Δz = 2 mm, Δx ~2 mm, Δy ≈ 2 mm, -3 cm < x < 3 cm, -1 cm < y < 1 cm, -15 cm + z_o <z < 15 cm + z_o.

4. Longitudinal scans of B_x and B_z; Δz = 2 mm; x = 0, y = 0, -3 m < z < 3m.

5. Longitudinal scans of single period coil measuring B_y and B_x. Signal captured in ≈ 2 mm increments, -3 m < z < 3 m.

4.3 Vacuum System

The vacuum system specifications for the U10.0 Undulator are driven by storage ring requirements. These include:

4.3.1 Aperture Requirements

The clear aperture for the U10.0 Undulator storage ring is a 60 mm horizontal by 19 mm vertical ellipse.

4.3.2 Vacuum Requirement

The vacuum specification is based on cross-sections for scattering of the electron beam by the residual gas and ions in the vacuum chamber [the elastic scattering cross-section is 2/3 of the total and the inelastic scattering is the remaining 1/3] and leads to a 10^{-9} Torr vacuum requirement at 1.5 GeV—400 mA operation after 40 A h of operation.

4.3.3 Diagnostics

Beam position monitors are required at both upstream and downstream locations on the insertion device vacuum chamber for locating the electron beam.

5.0 INSERTION DEVICE CONCEPTUAL DESIGN

The U10.0 Undulator mechanical design is very similar to the U5.0 undulator mechanical design shown in Figure 6.[9] The major subsystems identified are: the magnetic structure, which includes the hybrid pole assemblies mounted on pole mounts that are attached to the 4.5 meter long backing beams; the support and drive system, which includes the framework for supporting the magnetic structure and the mechanism for opening and closing the magnetic gap; the vacuum system, which includes a 5 meter long vacuum chamber and its associated pumping system; and the control system.

Fig. 6 The U5.0 Undulator

5.1 Design Philosophy

The approach taken for ALS insertion devices has been toward a generic design with the objective of reducing engineering and fabrication costs and for easier maintainability.

By subsystem, the following commonality exists between devices:

Magnetic Structure:

- Scaled undulator magnetic configurations,
- Similar backing beams for the undulators,
- Wiggler backing beam is a fractional length of the undulator backing beam

Support/Drive System:

- Identical support structures for the undulators,
- Identical drive systems for all devices,
- Support structure shortened for the wiggler.

Control System:

- Identical control systems for all devices.

Vacuum System:

- Similar vacuum chamber configurations for the undulators,
- Wiggler vacuum chamber similar to undulator but shorter,
- Identical pumping systems for the undulator vacuum chamber,
- Similar pumping system for the wiggler.

The design, fabrication, testing, and installation of the U10.0 Undulator will be very similar to the ALS U5.0 and U8.0 undulators.

5.2 Design Parameters

The following parameters in Table VII have been established for the U10.0 Undulator Conceptual Design.

TABLE VII. U10.0 insertion device engineering design parameters.

General	
Maximum peak field (at 2.335 cm magnetic gap)	1.05 T
Effective peak field (at 2.335 cm magnetic gap	0.98 T
Period length	10 cm
Number of periods	43
Number of full field poles	86
Magnetic Structure	
Overall length	456.4 cm
Pole width	8 cm
Pole heigth	9.4 cm
Pole thickness	1.42 cm
Number of blocks per half-period (one side of pole)	6
Entrance sequence	0, -1/4, +3/4, -1, +1, ...
End correction range (B_y)	1500 G cm
End correction range (B_x)	None
Multiple trim magnet range	± 3000 G cm
Support/Drive System	
Gap magnetic load (23 mm magnetic gap)	15,000 lbs.
Allowable gap variation (systematic)	140 μm
Gap range	2.335–21.6 cm
Gap opening time	1 min.
Minimum step resolution (1/10 of 5th harmonic)	2.8 μm
Maximum scan rate (1 bandwidth/sec)	2.10 mm/sec
Vacuum System	
Clear vertical aperture	1.9 cm
Maximum gap at pole windows	2.335 cm
Required pressure after 40 A-hr. of operation	10^{-9} Torr

5.3 Magnetic Structure

The magnetic structure includes the periodic magnetic structure, the end rotators, multiple trim magnets and the 4.5 m long backing beams.

5.3.1 Periodic Structure Magnetic Design.

The periodic magnetic structure consists of Neodymium-Iron-Boron blocks and vanadium permendur poles.[10] The configuration is conventional with a rectangular pole and Nd-Fe-B block array. A half period ($\lambda/2$) section of

the structure is shown in Figure 7. Generally, the principal objective of the design effort is to develop a magnetically well behaved structure which yields a high value of B_{eff} (as defined below) for mid-plane fields. The design approach utilizes 3-D hybrid theory and 2-D modeling with PANDIRA which is a sub-code of the POISSON Group of computer codes.[11] Here, the configuration was chosen to have the same transverse width as the U5.0 and U8.0 undulators for economy and still provide the necessary performance.

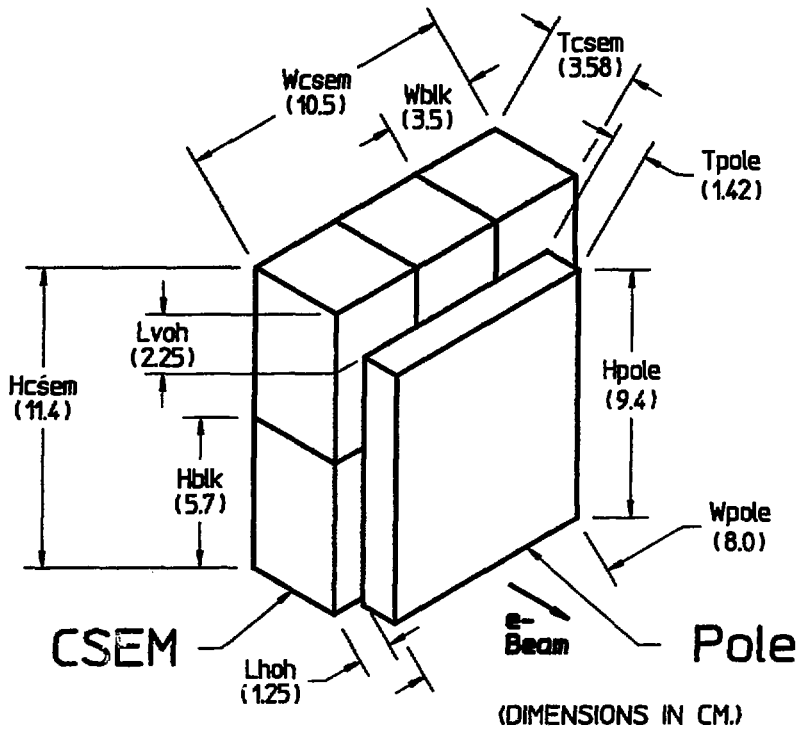

FIG. 7. Magnetic Structure—half period configuration.

5.3.1.1 Calculation of Structure

PANDIRA allows convenient 2-D modeling of anisotropic materials. The Nd-Fe-B characteristics are defined by the remanant and coercive field intercepts of the linear B-H curve along with its easy axis orientation angle. The vanadium permendur is described by a non-linear B-H curve which has been developed from measured data and is included in the input to PANDIRA.

2-D models are used to optimize the pole thickness, to provide detailed information about magnetic behavior and to provide flux information for the 3-D calculation. Vector potentials, which are the fundamental quantities calculated by PANDIRA, are used in detailed harmonic analyses and pole face investigations described below.

The optimum pole thickness is influenced by various parameters including saturation behavior of the pole material, operating point of the CSEM and ratio of gap to period and spatial harmonics in the magnetic field. All of these geometrical and magnetic properties are defined and utilized in the 2-D PANDIRA models which are used in the optimization of the pole thickness. For U10.0 this optimization process yields a pole thickness of 1.42 cm or pole thickness to CSEM thickness ratio of $T_{pole}/T_{csem} = 0.397$.

The transverse width of the pole is determined by external considerations such as constraint of dB_y/dx where x is the transverse direction (perpendicular to the beam). This dimension is 8.0 cm for the U5.0 and U8.0 undulators and is also used for U10.0. The starting point of the Nd-Fe-B above the pole face is determined by vacuum chamber and measurement constraints, as well as coercive field effects in the permanent magnet material near the pole tip.

Application of the 3-D hybrid theory is necessary for the design procedure since 2-D assumptions can yield configuration errors greater than 10%. The 3-D calculation separates the flux that enters and leaves the pole into what are called direct or B_r fluxes and indirect or scalar potential fluxes. The total direct flux for each pole is equal in magnitude to the total indirect flux associated with each pole. The direct fluxes come from the Nd-Fe-B and set the pole on a certain scalar potential. The indirect fluxes result from this scalar potential and are calculated for all surfaces and 2-D corners of the pole.

The final dimensions of the structure come from balancing of the direct and indirect fluxes, where overhang dimensions and pole height are manipulated to achieve desired performance and minimal volume of Nd-Fe-B. The overhang contributes to the direct flux and causes an increase in the scalar potential of the pole. For economy and to maintain similarity with the U5.0 and U8.0 undulators in the transverse dimension, the overhang of the sides of 1.25 cm is maintained. Calculations for U10.0 gave an optimum overhang on the top of the structure of 2.25 cm.

Calculations for U10.0 also yielded a pole height of 9.4 cm for a peak field of 1.05T and an effective peak field of 0.98T at a 2.335 cm gap.

5.3.1.2 Harmonic Content of Undulator Fields

Harmonic content is examined via Fourier analysis of the vector potentials calculated in 2-D by POISSON and PANDIRA. The periodic structure is assumed to be infinitely long and wide. The y-component of the fields in such a structure can be described by:

$$B_y(y,z) = B_1 \sum_{m=1}^{\infty} b_{2m+1} \cos[(2m+1)kz] \cosh[(2m+1)ky]$$

where $k = 2p/\lambda_u$, B_1 is the amplitude of the fundamental and $b_{2m+1} = B_{2m+1}/B_1$ is the normalized amplitude of the $2m + 1$ field component.

The third harmonic (b_3) at the mid-plane for the design pole thickness of 1.42 cm is 8.6% of the fundamental at the design gap of 1.4 cm, and decreases for larger gaps. Higher harmonics are negligible ($b_5 = 0.27\%$, $b_7 = -0.17\%$).

5.3.1.3 Performance Criterion—B_{eff}

Mid-plane field performance B_{eff} depends on the operating point of the Nd-Fe-B and the pole thickness (T_{pole}), where B_{eff} is given by:

$$B_{eff}^2 = B_1^2 + \frac{1}{3^2}B_3^2 + \frac{1}{5^2}B_5^2 + \ldots$$

5.3.1.4 Block Sorting

To achieve uniform pole excitation and reduction of integrated error fields, which affect the electron beam trajectory, block sorting is required for the U10.0 Undulator.

Figure 8 shows a partial view of the lower magnetic structure of a typical ALS undulator. The orientation of the permanent magnet blocks is parallel to the z-axis, i.e., parallel to the direction of the electron beam. The vanadium permendur poles can be seen between the magnet block arrays. The electron trajectory is shown schematically (with exaggerated amplitude) centered above the upper middle block of each magnet array. In the actual device, the structure is mirrored with opposite polarity above the electron beam trajectory.

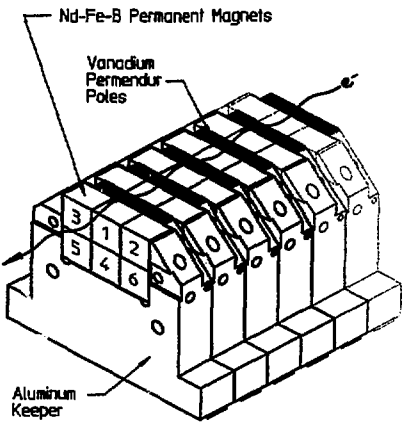

Figure 8. Partial view of lower half of undulator magnetic structure.

5.3.1.5 Sorting for Uniform Pole Excitation

In order to establish uniform pole excitation, it is necessary that the average magnetic moment in the direction of magnetization, $\overline{M}_2$, for the magnet array associated with any pole, be the same as that of any other array. The first step of the sorting algorithm is to arrange blocks into groups of six using this $\overline{M}_2$ criterion.

For the U10.0 undulator, the moment values of the magnet block populations are determined by automated Helmholtz coil measurement. Values of M_x, M_y, and M_z are recorded to an electronic file. The data are then arranged in ascending values of a criterion called Γ_i calculated for each block, where:

$$\Gamma_i = M_{xi}^2 + M_{yi}^2 \quad \text{for } i = 1 \text{ to } n \tag{1}$$

where n is the total number of blocks being sorted. The Γ criterion associates a combined minor component magnitude with each block. Blocks with lower Γ values are preferred for positioning close to the electron beam.

This ordered group is then subdivided into six subgroups with group one having the lowest Γ values, group two having the next lowest Γ values and so on. Each of the six groups is assigned a position in the six block magnet

arrays as shown by the numbering scheme on the magnet blocks in Fig. 8. Thus, any block from group one is constrained to a position immediately under, or above, the electron beam.

The next stage of the sorting process is to construct the six block magnet arrays. The objective here is to establish uniform averaged M_z values for the final six block arrays. This is done using a non-iterative ordering and pairing technique which is a feature of the sorting code INSORT[12]. The steps of the process as applied to a population of *n* blocks are as follows:

1. The global average of M_z for the entire block population is calculated and the deviation from that global average (dM_z) is calculated for each block.

2. The six groups, described above, are then monotonically ordered in ascending values of dM_z.

3. Groups one, two and three are searched for the block having the greatest absolute value of dM_z.

4. The two groups which did not contain the block selected in Step 3 (above) are searched for the block having the greatest magnitude of dM_z of the opposite sign of that of the step 3 block.

5. The blocks selected in steps 3 and 4 (above) are paired and their dM_z values are averaged. They are also removed from the data set and stored along with their average dM_z value and group affiliations.

6. Steps 3–5 (above) are repeated *n*/3 times which results in *n*/3 paired blocks and *n*/3 single blocks.

7. The *n*/3 pairs are monotonically ordered by their average dM_z values and the single blocks are monotonically ordered by their dM_z values.

8. The ordered pairs and single blocks of step 7) are then paired by opposite extremes. The average dMz value of each of the resulting triplets is then calculated.

9. Steps 3–8 (above) are repeated for blocks in groups 4, 5, and 6.

10. The group 1-2-3 triplets and group 4-5-6 triplets are separately ordered monotonically by their average dM_z values and paired by extremes to form the final six block arrays.

The above algorithm results in very rapid reduction in deviation from global average of M_z values for typical magnet block populations used in hybrid insertion devices.

When applied to a block population having an initial deviation of 4% for single blocks for a previous insertion device, the algorithm resulted in a final maximum deviation from global average at the six block array stage of less than 0.02% which is below current, practical, measurable levels.

5.3.1.6 Sorting for Reduced Integrated Field Errors

Extensions to the above described algorithm will be used to minimize the effects of minor component errors (M_x, M_y) on electron trajectories. A large parameter space for optimization remains after the sorting algorithm described in Section 5.3.1.5 is applied.

Parameters such as block rotation and position shifts within six block arrays as well as relocation of arrays in the magnetic structure will be used in conjunction with measured information about block minor components to

develop field integral objective functions. Iterative optimization techniques such as synthetic annealing will be used to minimize these objective functions.[13]

5.3.2 End Magnetic Structure Design

To avoid steering perturbations of the beam as it travels through the insertion device, it is necessary to control the configuration of the fields at the ends.

Because of concerns about dimensional instability caused by coil heating effects, no end coils are used in this design. Instead, the basic end pole design utilizes a system of Nd-Fe-B rotors for fine tuning.

The U10.0 end structures represent a refinement of the ALS U5.0 and U8.0 insertion devices end designs. Like those devices, the U10.0 device uses a system of Nd-Fe-B rotors to tune the field distribution at the ends of the insertion device.

The entrance scheme for the device consists of a nominal, normalized scalar potential distribution of 0, .25, -.75, 1.0, -1.0, ... etc. The device has an even number of poles which implies an exit scheme with the same scalar potential magnitudes but with the opposite signs.

Fig. 9. is a longitudinal cross-section of the end of the magnetic structure installed on the backing beam with a connecting magnetic shunt. The pole indexing convention is given in this figure with the first or field clamp pole designated as pole "0," the second as pole "1," and so on.

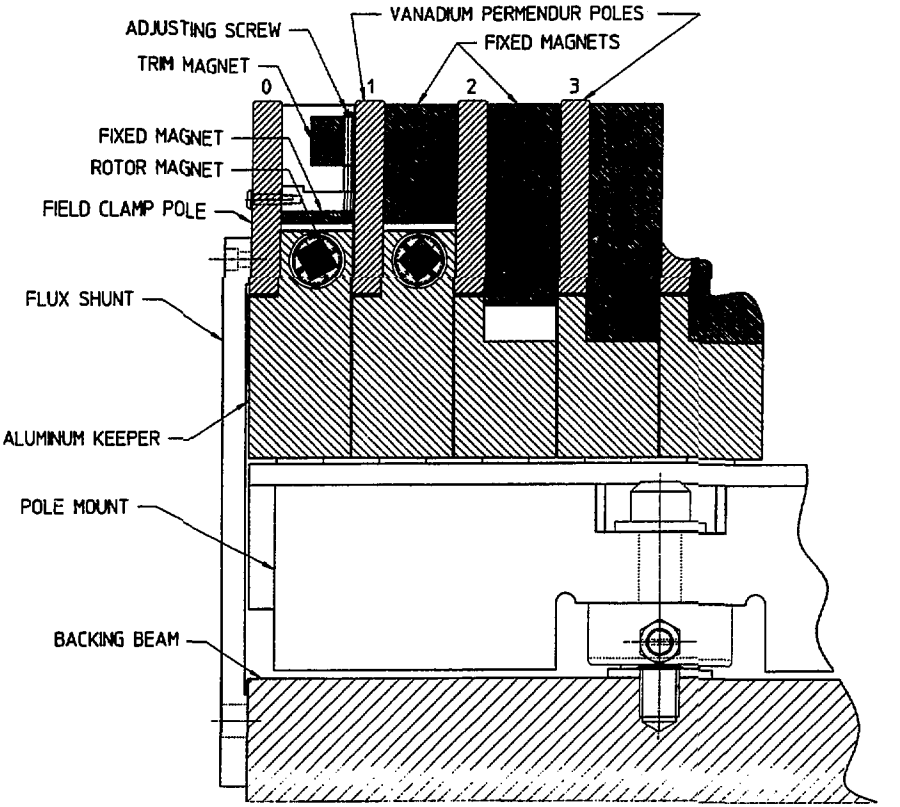

FIG. 9. U10.0 Undulator end magnetic structure.

Between the poles in this figure is shown a combination of fixed and moveable permanent magnet material. Easy axis orientations of the permanent magnet blocks are also shown for a hypothetical 'tuned' case.

The volume of the fixed material between poles 0 through 3 is selected via 3-D numerical modeling to produce the 0, 1/4, -3/4 normalized scalar potential distribution mentioned previously. From pole 3 on, the volume of the permanent magnet material is uniform until the opposite end of the device is reached. The opposite end of the magnetic structure has the same permanent magnet volume distribution but with opposite order and polarity.

5.3.3 Multiple Trim Magnets

Multiple trim magnets will be designed into the end structures to reduce the higher order fields to meet the accelerator requirements in integrated magnetic field errors.[14]

Application of the multiple trim magnets on the U5.0 and U8.0 undulators has demonstrated better than an order of magnitude reduction of both the normal and skew integrated magnetic field errors.

A flux plot of a trim magnet in an insertion device structure is shown in Figure 10. The field produced at the midplane by the trim magnet may be varied by adjusting the size, position and orientation of the magnet. To correct integrated magnetic field errors in the device aperture, a transverse array of these trim magnets is used.

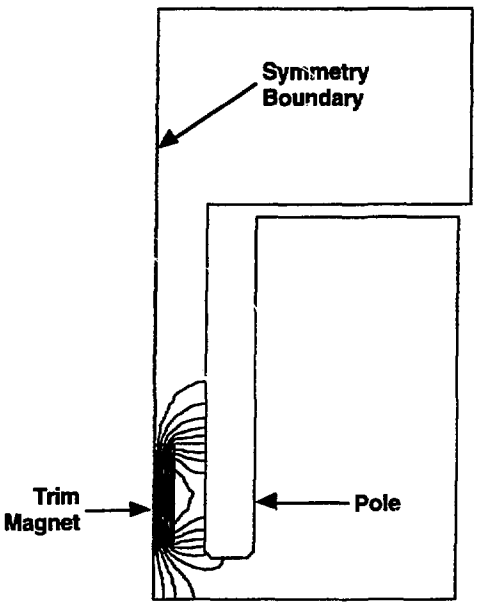

FIG. 10. Flux plot of a single trim magnet in an insertion device.

5.3.4 Periodic Magnetic Structure Mechanical Design

The basic building block of the periodic magnetic structure is the half period pole assembly, which consists of an aluminum keeper, a vanadium permendur pole, and 6 Nd-Fe-B blocks, and is shown in Figure 11.

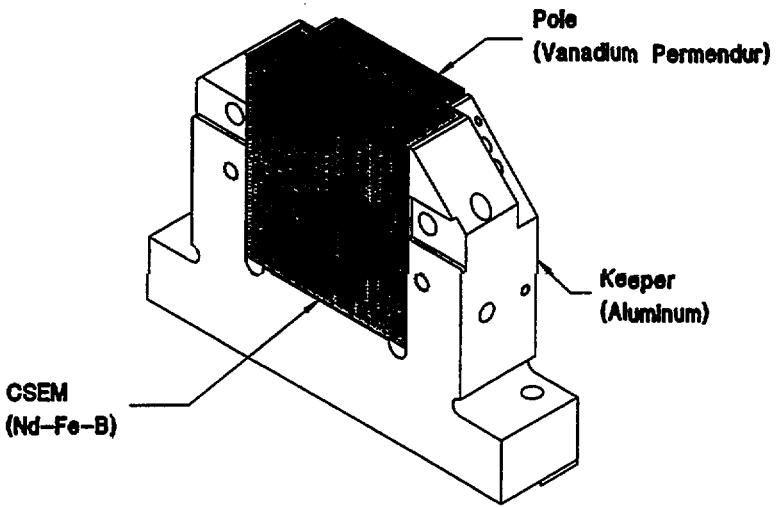

FIG. 11. U10.0 half period pole assembly

The vanadium permendur poles will be machined, heat treated and then finish ground. Each pole will be pinned to its keeper with four stainless steel pins and secured with two stainless steel screws. All the pole and keeper assemblies will have a final trimming grind on the back of the keeper so that the overall height of all these assemblies will be within 25 μm. A simple dowel pin will be provided in the back of each keeper, combined with a close keeper thickness tolerance and precision spacers, to provide the required half period spacing of each half period pole assembly on the pole assembly mount.

For the U10.0 Undulator, 1,020 full-size Nd-Fe-B blocks and 60 smaller Nd-Fe-B blocks are required. To account for block breakage, blocks that do not meet specifications, incorrectly assembled and damaged pole assemblies, requires the purchase of about 6% extra blocks or 1,144 blocks total.

The Nd-Fe-B permanent magnet blocks for U10.0 are to be ordered per LBL Specification, M793.[15] Key sections in Specification M793 include:

Magnetic Properties:

2.1 A nominal coercive force of 10.6 kOe after thermal stabilization ~ at 25° C.

2.2 A nominal intrinsic induction, that is linear within 2.5% to at least 120% of the nominal coercive force at 50°C after thermal stabilization.

2.4 Blocks thermally stabilized at 60° C for 3 hours.

2.5 The direction of magnetization, easy-axis, to be within ± 3°.

Mechanical Properties:

3.1 Block dimensions are 35.64 mm thickness [direction of magnetization] x 35.00 mm width x 57.00 mm length. Thickness tolerance is ± 0.050 mm. Width and length tolerances are ±0.25 mm.

Coating Information:

4.1 Blocks to be suitably coated with a metallic coating, thickness at least 0.010 mm and not to exceed 0.030 mm, to prevent corrosion in a 25° C, 75% relative humidity environment.

Packaging:

6.1 Blocks are to be shipped in foam cubes, 10 cm on a side, to make subsequent handling at LBL easier.

The Nd-Fe-B blocks will be inserted into the pole assembly using a block holder and then held in place with a bonding fixture. The adhesive will be cured at room temperature.

The secondary building block of this design will be the assembly section. Half period pole assemblies will be mounted onto the pole mounts. The support points for the pole mounts will be located to achieve minimum deflection due to the magnetic loading on the pole mounts. The length of these mounts is determined by the allowable deflection due to the magnetic loading. For those used in the U10.0 Undulator, the maximum length is approximately 93 cm. The mating surface of the pole assembly mount to which the half period pole assemblies are fastened will have a flatness of 12 μm. To achieve the target 25 μm pole height variation on an assembly section will require shimming between the half period pole assemblies and the pole mount. The U10.0 undulator assembly section will look similar to the U5.0 undulator assembly section shown in Figure 12.

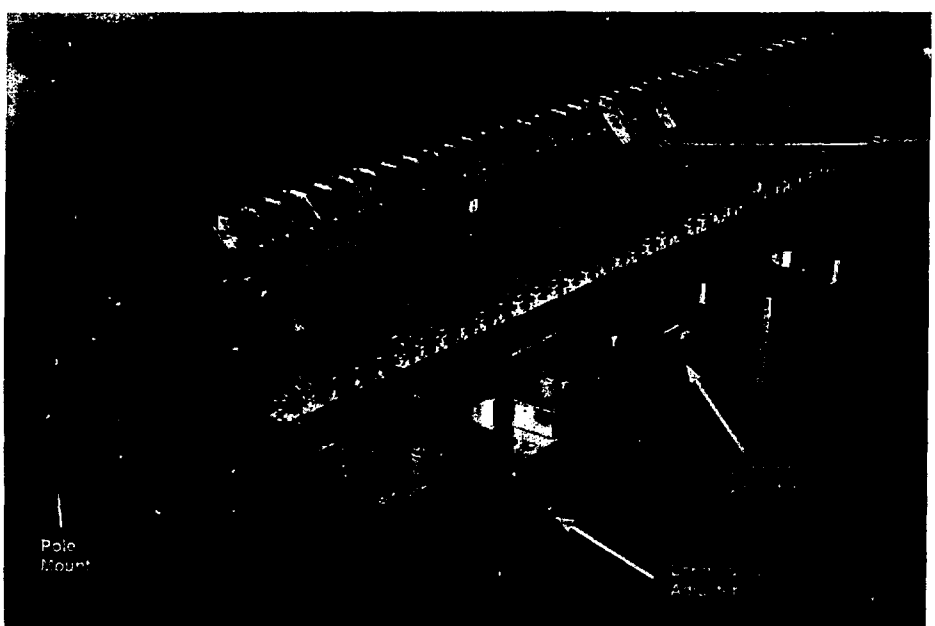

FIG. 12. U5.0 Undulator assembly section.

5.3.5 End Structure Mechanical Design

In the previous devices the end pole assemblies were placed on a separate pole mount and formed independent magnetic structure modules. In the current design, the end pole assemblies are incorporated into the ends of four of the ten large magnetic structure modules which comprise the entire magnetic structure of the device.

Another departure is the simplification of the rotor drive system used for the previous devices. The former arrangement incorporated a secondary shaft and chain drive system as well as an elaborate external control and locking mechanism.

Figure 13 shows the current mechanical arrangement which consists of two rotors on each module which are designed to be adjusted by means of a simple removable hand drive or wrench and which have a compact locking system at the end of each rotor. This locking mechanism is designed to be pinned to fix the rotor position after final rotor adjustments have been made.

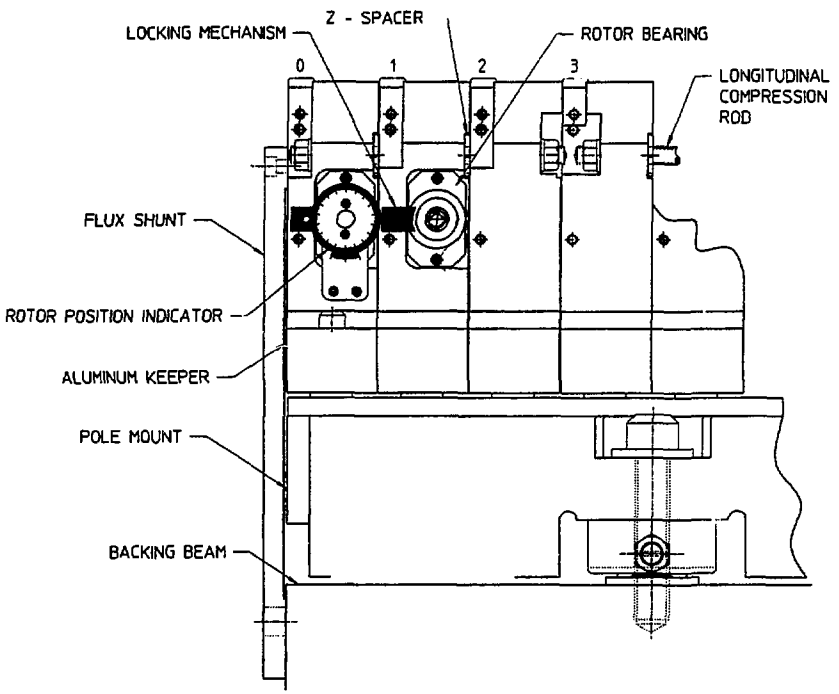

FIG. 13. End rotor mechanical layout.

The vertical position of the rotors is such that a direct shaft drive may be coupled to the rotors without interfering with the vacuum chamber. This capability, if needed, is necessary to install a motor drive for remote rotor position control during normal operation of the insertion device.

The three end pole assemblies are connected with a separate set of longitudinal compression rods than that used for the rest of the pole assemblies on that module. This allows the removal of these pole assemblies for maintenance or to adjust the permanent magnet quantities without disturbing the alignment of the rest of the module.

The rotor position indicator is also shown in figure 13. This is a simple dial which is directly attached to the rotor housing itself. With the exception of direct motor drive, all rotor functions (driving, locking and position indication) can be performed on the aisle side of the insertion device.

Figure 14 is a transverse cross-section of the end structure between pole 0 and pole 1. The trim magnet array can be seen as well as the rotor housing and bearing arrangement. As in previous designs, these housings can be easily removed to change the quantities of permanent magnet material. This allows their tuning capacity and sensitivity to be adjusted. Also shown in this figure is the array of fixed magnets which are the primary source of excitation at this location in the end structure.

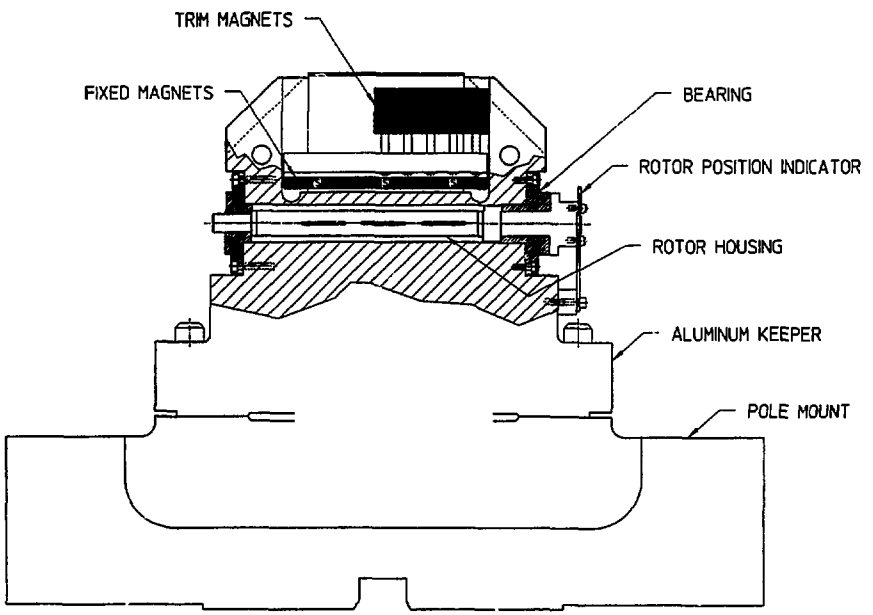

FIG. 14. End rotor, end view.

5.3.6 Multiple Trim Magnets Design

The correction of the higher order integrated magnetic field errors is with the multiple trim magnets. The U10.0 multiple trim magnet configuration will be similar to that developed for the U5.0 undulator which is shown in Figure 15. To change the field integrals, the trim magnets can be adjusted vertically up or down, or they can be replaced with different size trim magnets.

Fig. 15. U5.0 Undulator multiple Trim Magnet Array.

5.3.7 Field Error Corrections Design

To reduce the effect of environmental fields, flux shunts are used, which carry a substiantial portion of the external environmental fields between the upper and lower backing beams[16], as shown in Figure 16. The flux shunts (six) are nickel, non-low-reluctance linkages which magnetically connect the upper and lower backing beams together.

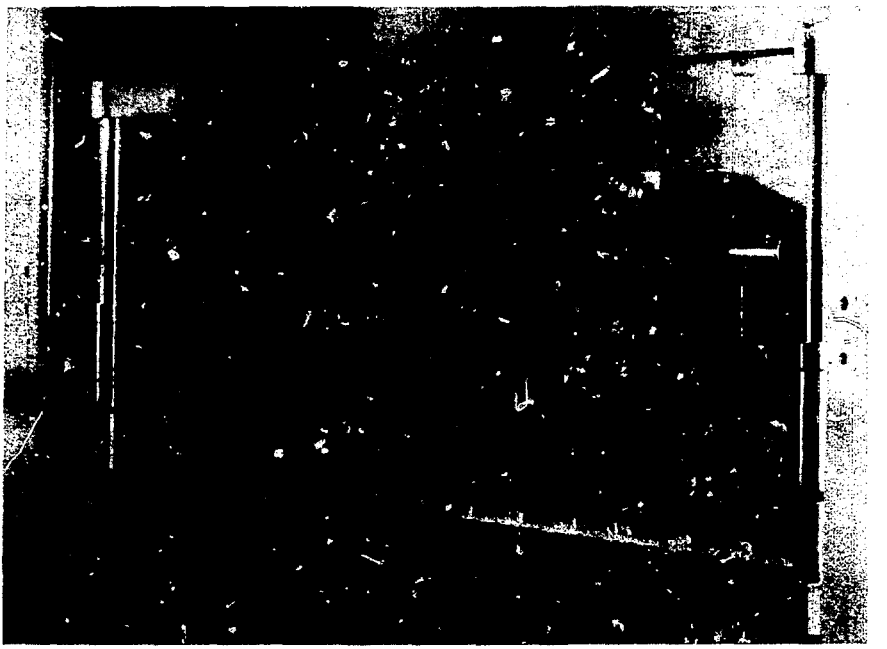

Fig. 16. U5.0 Undulator flux shunts.

Additional capability is provided for correcting local steering errors by either adding permanent magnet or iron shims symmetrically to pole pairs to produce local steering fields. Two cylindrical holes and two slots are provided in each keeper assembly, close to the pole face, which extend to the pole where permanent magnet material, or iron, can be positioned as a backup to shimming, tuning coils can be designed into the magnetic structure in the event that difficulty is encountered in achieving the required field performance.

5.3.8 Backing Beam Mechanical Design

The backing beam, shown in Figs. 6 and 17, will be a skirted-box section design with a very rigid moment of inertia to length ratio resulting in minimum deflection due to the magnetic load on the backing beam. The backing beam will be a welded steel construction. To minimize material creep, the welded backing beam will be rough machined, stress relieved, and final machined. The support points for the backing beam will be located to achieve minimum deflection.

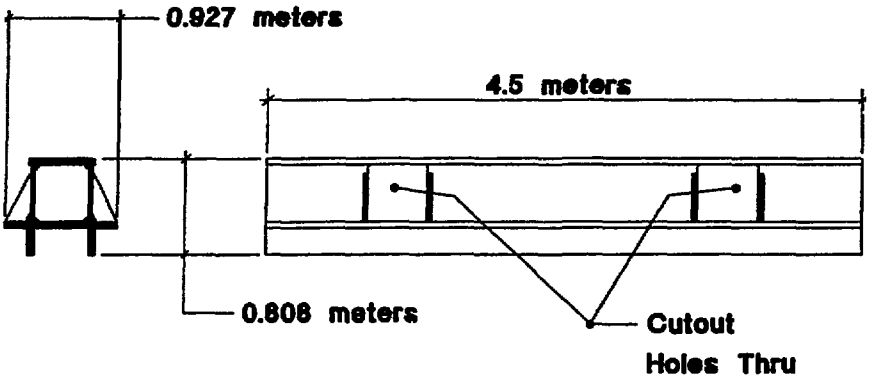

FIG. 17. Backing beam configuration.

From the allowable systematic gap error of 140 μm, an allowable backing beam flatness variation is determined as half of the gap error, or 70 mm. Errors that contribute to this backing beam distribution include the backing beam deflection due to magnetic load, thermal distortion, assembly section mounting and the drive system gap reproducibility (see Section 5.5.2).

Backing beam deflection calculations, carried out for the U5.0 Undulator magnetic loading and scaled for U10.0 Undulator, give the follow results:[17]

Deflection of beam without cutouts	2.2 μm
Additional deflection due to cutouts	0.8 μm
Additional deflection due to support location errors	0.7 μm
Total deflection due to magnetic loading	3.7 μm

Deflections of the beams due to their own weight, provided they are equal, do not affect the gap variation.

Deflections due to a vertical temperature gradient in a backing beam are of more concern. These deflections are:

- 3.4 μm/0.1 degree C at the center of the beam.
- 7.8 μm/0.1 degree C at either end of the beam.

To minimize deflections due to vertical thermal gradients will require good vertical circulation of the air at the insertion devices. Fortunately, the thermal time constant of the backing beams is long—24 hours—compared to a typical photon run of 8 hours, and can be increased to 40 hours with the addition of a 1/2 inch layer of Ensolite foam.

The backing beam error budget is given in Table VIII.

TABLE VIII. Backing beam error budget.

	μm
Backing beam deflection due to magnetic loading	3.7
Thermal distortion allotment	49.3
Assembly section alignment tolerance	12.0
Drive system half-gap reproducibility	5.0
Allowable backing beam flatness tolerance	70.0

5.3.9 Magnetic Structure Alignment

Magnetic structure alignment is carried out using techniques developed during the assembly of the U5.0 and U8.0 Undulators.[18]

As previously mentioned the vertical and longitudinal alignment tolerances for the poles of these structures are 25 μm and 38 μm respectively over the entire 4.6 m length of the device. To meet these tolerances, the assembly sections (modules) are first individually aligned using an automated coordinate measurement machine (CMM) and shimming techniques. The longitiudinal alignment of the pole assemblies are performed using longitudinal spacers and compression rods shown in figure 18.

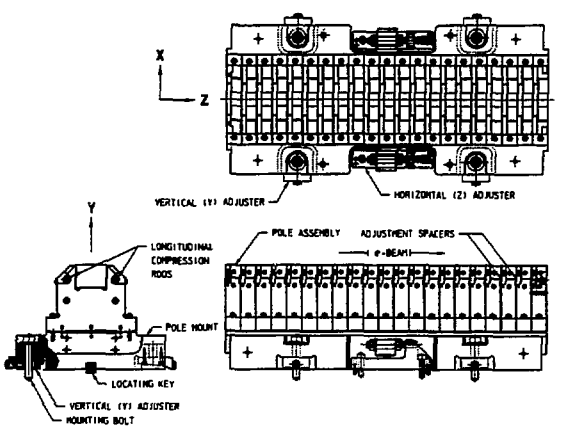

FIG. 18. U10.0 Undulator assembly section.

The vertical pole positioning is performed by placing pre-cut metal shims between the keeper base pads and pole mount surfaces. This is an iterative process due to the non-linear nature of this type of mechanical system. Averaging and three dimensional linear least squares fitting techniques are applied to CMM measurements of

the modules to establish statistically based error reference planes. Graphical spread sheets are used to create representations of vertical and longitudinal pole position errors for this phase of the alignment process. A representative plot for a module is shown in figure 19.

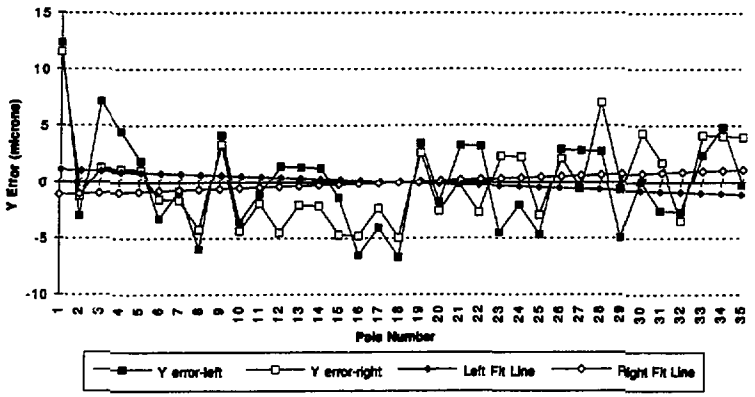

FIG. 19. Vertical (Y) pole position error graph.

These pre-adjusted modules are then installed on the backing beams and aligned relative to each other using laser interferometer techniques. The longitudinal positions of all poles of each module are measured using a simple linear interferometer and associated optics. Because of the differential expansion coefficient between the aluminum modules and steel backing beam, a bilinear temperature compensation function is applied to the position data to predict periodicity errors at a pre-determined operating temperature (that of the storage ring tunnel) which in general differs from ambient temperature at the alignment site.

Vertical alignment of the periodic modules is performed by generating vertical pole position error profiles of the full 4.6 m structures. These profiles are obtained by using an angular interferometer and performing an integrated angle calculation on the data. A typical plot for an entire 4.6 m modular assembly is shown in figure 20. Least squares fit planes for each module are calculated and used in making differential vertical and angular adjustments. Repeatability error for these measurements is typically less than 3 μm (.00012 in).

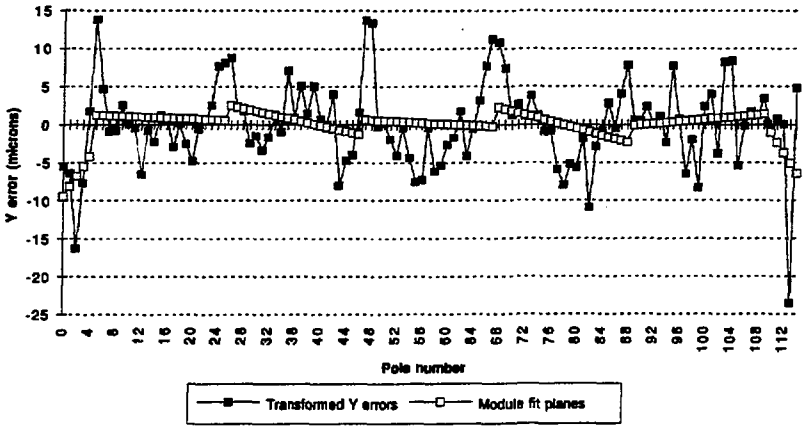

FIG. 20. Laser interferometer vertical (Y) error profile w/ least squares error plane for each module

The actual adjustment of the modules will be performed using the vertical and longitudinal adjustment mechanisms shown in figures 21 and 22. Dial indicator arrays will be used to confirm that adjustments comply with the differential movements indicated by the above error profiles.

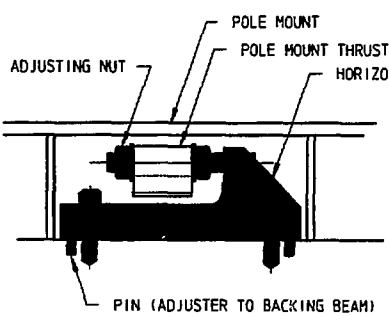

FIG. 21. Longitudinal (Z) adjuster.

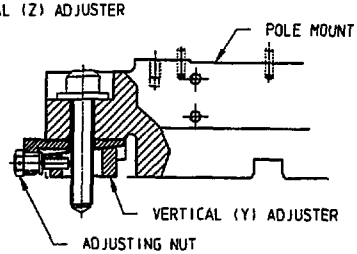

FIG. 22. Vertical (Y) adjuster.

5.4 ID Magnetic Measurement Facility

Two general types of measurements are needed for insertion devices: 1) block measurements for determining the magnetic characteristics of the Nd-Fe-B blocks, and 2) insertion device measurements for mapping the fields of the entire device.

Block measurements include mechanical measurements and determining the major and minor axes magnetic moments with a Helmholtz Coil System.[19,20] Full insertion devices are measured with the Insertion Device Magnetic Measurement Facility (IDMMF) which can utilize Hall probes, point coils, one period length coils and multi-period coils.[21] The IDMMF is a high speed, precision magnetic measurement facility. It is capable of completing a 2500 sample, 6 m scan with precision axial position monitored using a laser interferometer in under one minute to determine local and integrated field information. In addition, (as a check) a 5.5 m long 1 cm wide coil is used to measure the field integral through the entire insertion device.

5.5 Support/Drive System

The support/drive system includes the support structure that provides the framework for holding the magnetic structure and drive train and the drive system, which will open and close the magnetic gap. The U10.0 Undulator Support/Drive System is the generic ALS Support/Drive System, and thus, almost identical to the U5.0 and U8.0 Undulator Systems. Below is a description of that system.

5.5.1 Support Structure Design

The support structure is designed to support a maximum magnetic load of 84,000 lbs, the loading due to a 1.85 T field, 10 cm wide pole in a 5 m long undulator, which is adequate for the U10.0 Undulator. The support structure design developed is compatible with the storage ring tunnel and the adjacent beamlines. It can accommodate the vacuum system and has an alignment method and a floor support system.

The support structure design of the U5.0 Undulator (U10.0 Undulator support structure is identical) is shown in Figures 6, 23, 24, 25, and 26. Building from the floor, the support structure consists of a base onto which two horizontal beams are mounted, then four vertical posts are mounted—and lastly—the two remaining horizontal beams. The four horizontal beams carry the backing beams of the magnetic structure. These horizontal beams are inserted through the webbing of the backing beams to minimize the overall height of the support structure to less than 8 feet. (As previously explained in Section 5.3.8, these cutouts in the webbing of the backing beams only cause small additional beam deflection.)

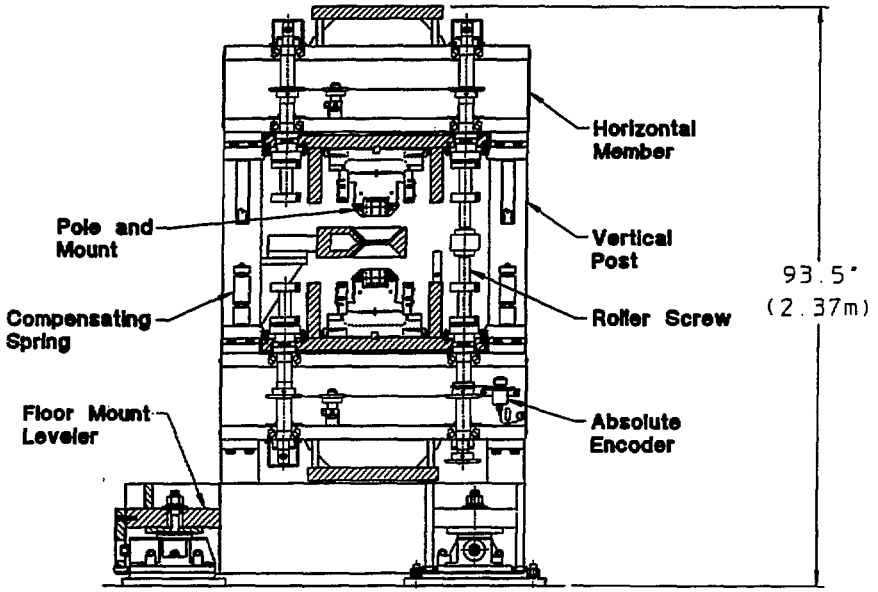

FIG. 23. Undulator end view.

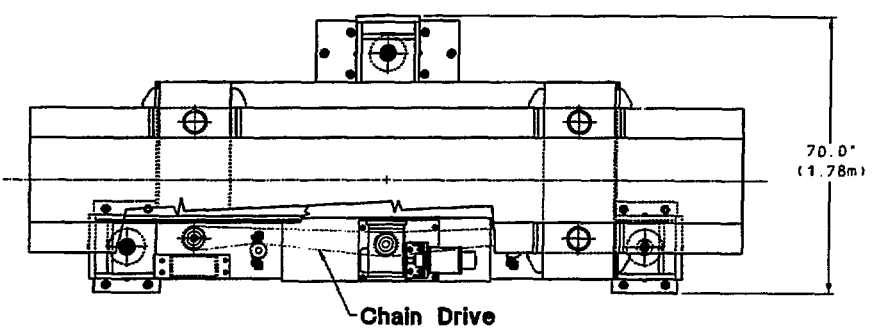

FIG. 24. Undulator plan view.

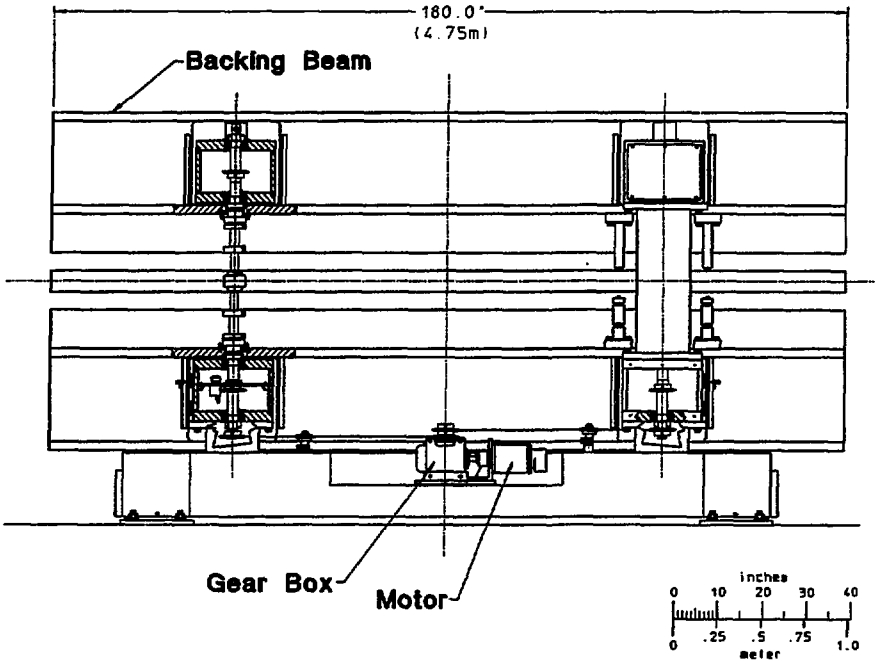

FIG. 25. Undulator elevation view.

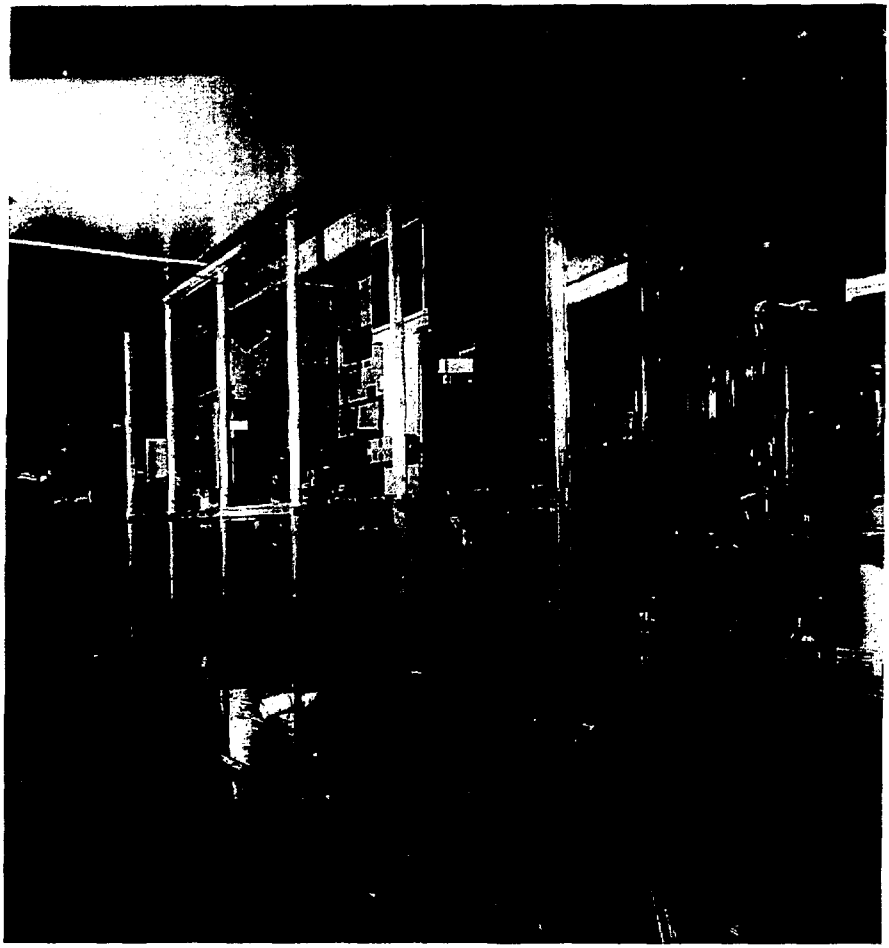

FIG. 26. Undulator installed in storage ring.

The base is a welded assembly containing three *y*-axis leveling mounts for a kinematic support system. The *x* and *z* axis adjustments are also provided at each leveling mount. This arrangement provides a limited but satisfactory range of adjustments for alignment in all six degrees of freedom needed for installation and alignment.[22]

The four vertical posts and four horizontal beams are bolted together and to the support frame. This modular arrangement allows for ease of fabrication, installation, calibration and servicing.

All subassemblies are stress-relieved before final machining to minimize material creep.

During assembly, survey fiducials are placed on the four vertical posts and various other surfaces to facilitate installation alignment of the undulator in the storage ring. Either optical tooling survey alignment or ALS coordinated surveying system will be used for the final alignment. Periodic leveling to accommodate ground settling will use the same y-axis leveling mounts.

A magnetic load compensating spring system will be provided to buck the gap dependent magnetic load similar to that used on the U8.0 Undulator.[23] The system will utilize eight assemblies of two different compression springs set in-line with appropriate stops to match the magnetic load to within 20% of the a 15,000 pound magnet load at a 23 mm gap.

The compensating spring system provides the following advantages:

1. Reduced system friction, which gives better positional response from the drive system.

2. No motor load holding torque required at any magnet gap, which gives stationary stability when the null position is reached. Motor current can be turned off or reduced to minimize motor heat-up.

3. Elimination of "lifting" when the magnetic load exceeds the gravitational beam weight of the lower backing beam.

4. Reduced structure compression, which gives better gap reproducibility.

5.5.2 Mechanical Drive System Design

The drive system design capabilities include opening the magnetic gap with an 84,000 lbs magnetic load; a step resolution <1.02 μm (based on 1/10 of the 5th harmonic of U3.65 undulator); a velocity >2.31 mm/sec (based on a scan rate of 1 bandwidth/sec for an 11 cm period device). Interfacing with the control electronics allows both local and remote control. The magnetic gap range will be 2.3 cm to 21.6 cm.

Various aspects of the drive system are shown in figures 23, 24, 25, 27, and 28. The backing beams are supported by the Transrol roller screws. These roller screws are in turn, all connected together with a system of roller chains, sprocket wheels and spring-loaded idler sprocket wheels. A gearbox and a stepper motor drive the system. An absolute rotary encoder is coupled to a Transrol roller screw shaft to read the absolute position of the magnet gap.

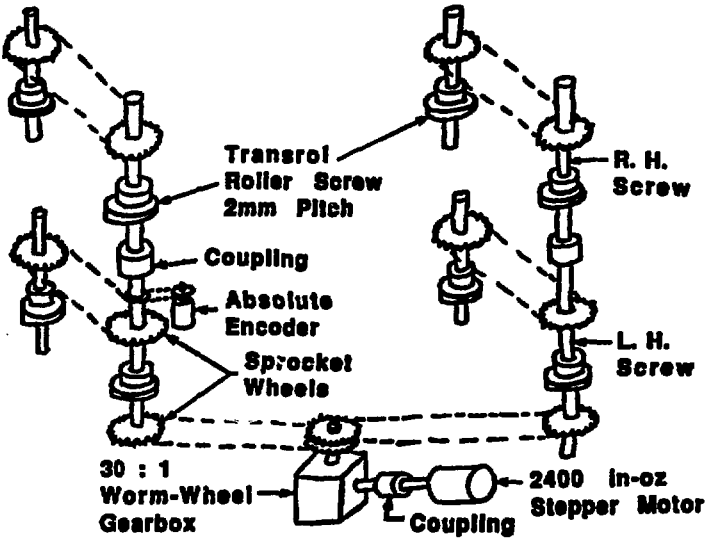

FIG. 27. Undulator drive system schematic.

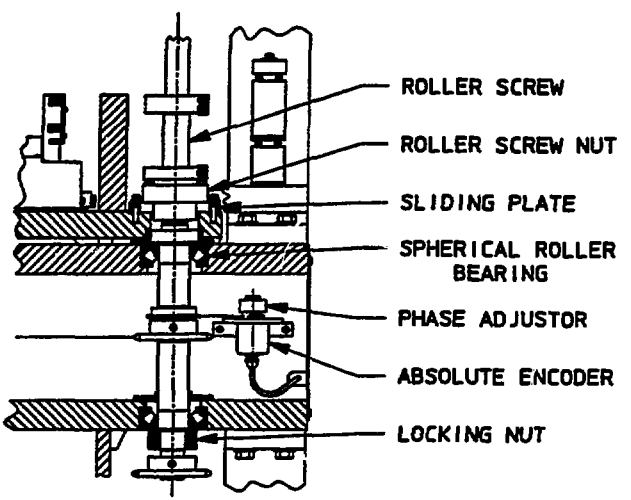

FIG. 28. Transrol roller screw layout.

The roller screws are supported on spherical bearings mounted in the support structure horizontal members. Four right-handed roller screws on the upper section and four left-handed roller screws on the lower section coupled by shaft couplings and roller chains and sprocket wheels combine to provide equal but opposite vertical motion of the upper and lower backing beams. This system is coupled to the gear box by roller chains and sprocket wheels. The stepper motor is connected to the gear box by a flexible coupling.

The drive system has been sized to drive the system under maximum magnetic load (minimum gap), even though compensating springs are used to buck the magnetic load (see Section 5.4.1). The roller screw will have a 2 mm pitch. Since there will be upper and lower roller screws the total pitch change will be 4 mm/revolution. The gear box has a 30:1 reduction unit. The stepper motor has 200 steps per revolution. A selection of 10 micro-steps/step by the control electronics for the stepper motor will provide 2,000 steps/revolution operation and result in a gap resolution of 0.07 μm. At 2000 steps/revolution operation, the motor can easily be driven at a velocity to move the gap from full closed to full open in approximately one minute. The stepper motor is capable of moving the gap for step scans at the rate of one bandwidth/second. For an 11 cm period insertion device, this translates into a maximum gap change rate of 2.3 mm/second.

An absolute encoder is coupled to one roller screw shaft by means of a Flex-E-Gear drive with a 4:1.75 step-up ratio. The encoder selected has a resolution of 16,384 word counts/revolution. This combination will read out to a resolution of <0.1μm. A harmonic drive phase adjuster is used to calibrate the gap to the encoder readout.

Analysis of the proposed drive system design yields the following: the gap position uncertainty due to stick-slip is < 0.4 μm. Backlash is estimated at 87 μm in gap motion, which requires unidirectional scanning and control of the undulator gap.[24] With unidirectional scanning, the scan-to-scan gap reproducibility is estimated to be within 11 μm. Calibration test on the U5.0 Undulator show gap reproducibility is within ± 5 μm.[25]

Protection for the drive system is as follows:

1. Open-loop control system with preset limits for travel stored in the computer program.
2. Micro-switches for minimum and maximum gap positions hard-wired to the control system.
3. Mechanical stops for minimum and maximum gap positions.
4. Stepper motor can be stalled at full torque current.
5. Mechanical drive components are designed to handle full stepper motor torque.
6. Full load current sensing in the control system for shut down after a preset time interval.

5.5.3 System Assembly

The Support/Drive System is first assembled without the magnetic structure installed, then disassembled, the magnetic structure then installed into backing beams and lastly, the system is reassembled with the magnetic structure installed in the backing beams. This procedure allows for careful alignment of the support and drive systems without the complication of installed magnetic structures.[26,27] Final pinning of the support structure is done after the magnetic measurements are completed. A PIR follows the Support/Drive System assembly and pre-installation work of the undulator.[28]

Results of tests carried out with the control system on the completed IDB-U5.0 support structure/drive system are tabulated in Table IX, and demonstrates that the system requirements have been met.

Table IX. Support, drive, and control system test results.

Test	Performance
Magnetic structure alignment (upper structure with respect to the lower structure)	Gap parallelism within 5 μm,transverse within 250 μm longitudinal within 150 μm.
Gap range	14 mm to 210 mm
Gap opening-closing time	1 minute
Absolute accuracy	Within ± 5 μm
Backlash (encoder to gap)	Within 10 μm for bi-directional motion
Scan rate	3.33 mm/sec maximum

Magnetic field taper can be provided manually by stepping one of the main roller chain sprockets with respect to the chain in increments of 87 μm/sprocket tooth.

5.5.4 Local Temperature Control

It is important that the insertion devices be maintained at a constant temperature during a photon run, typically eight hours duration. A uniform change in temperature of the device will cause a shift in the energy spectrum. A vertical temperature gradient in the backing beam will cause a broadening of the spectrum.

With a uniform change in temperature of 1 degree C of an insertion device and operating at small gaps, the energy shift will be 0.2%. With the tunnel air temperature controlled to ±1 degree C and the thermal time constant of the magnetic structure 24 hours, the maximum temperature change that the magnetic structure would experience would be 0.5 degree C in an 8 hour period which would result in an energy shift of 0.1% which is acceptable.

Further broadening of the spectrum will further occur if the vertical temperature gradient in a backing beam exceeds approximately 0.1 degree C. To prevent a temperature gradient from being established in the backing beam requires that the surrounding air be uniform in temperature. This is accomplished by circulating the air within an insertion device enclosure. Air will be moved with muffin fans, located within the enclosure.

To protect the magnetic structure from damage due to excessive temperature rise, a temperature interlock system will be built. The backing beam and tunnel temperatures will be continuously monitored. First, an alarm condition will be registered in the control room at 28 degrees C, then at 29 degrees the interlock chain for the major power supplies (which are the heat sources) will be tripped.

5.6 Insertion Device Control System

The insertion device control system (IDCS) has been designed to provide a general drive system which will accommodate the full compliment of insertions devices at the ALS in terms of accuracy, resolution, speed, and maximum lifting capability. The original requirements were to created a system that could:

— lift a 84,000 pound load,

— transverse 210 mm of gap motion,

— complete a full open-to-close transition in less than five minutes,

— absolute positioning accuracy of ± 1 μm,

— minimum scan speed of less than 1.0 μm/sec,

— maximum scan speed greater than 2.31 mm per second, and

— provide a convenient method of controlling the gap position from the control room and experimental stations.

To date, these requirements have been met, with the exception of the ± 1 μm positioning accuracy with the IDCS.

Shown in Figure 29, is a schematic of the IDCS, a stepper motor system from Compumotor. To date, three identical device control systems have been built for the U5.0 and U8.0 undulators. The IDCS for the U10.0 will be nearly identical with the exception being the addition of an incremental encoder.

The motor is capable of micro-stepping at 2000 steps per revolution which corresponds to .0667 microns of gap motion per step, at a maximum velocity of 25 revolutions per second, which corresponds to a gap velocity of 3.33 mm per second. The indexer coordinates the entire drive system. It has a unique language called X-language (developed by Compumotor). The system is controlled by sending a sequence of X-lanquage commands to the indexer over an RS-232 link. This can be done using an ILC, or any other computer with an RS-232 port. The Compumotor AR-C absolute rotary encoder has 16,384 steps per revolution, which corresponds to 0.107 μm of gap motion per step. Using a calibraton table, the encoder provides the absolute position of the insertion device gap as well as a software limit switch to protect the vacuum chamber from being punctured by the magnetic pole tips. A second level of protecton is provided using micro-switches. If an opening, or closing, limit is detected, the indexer rapidly decelerates the backing beams. If this system fails, then a mechancial hard stop will protect the vacuum chamber.

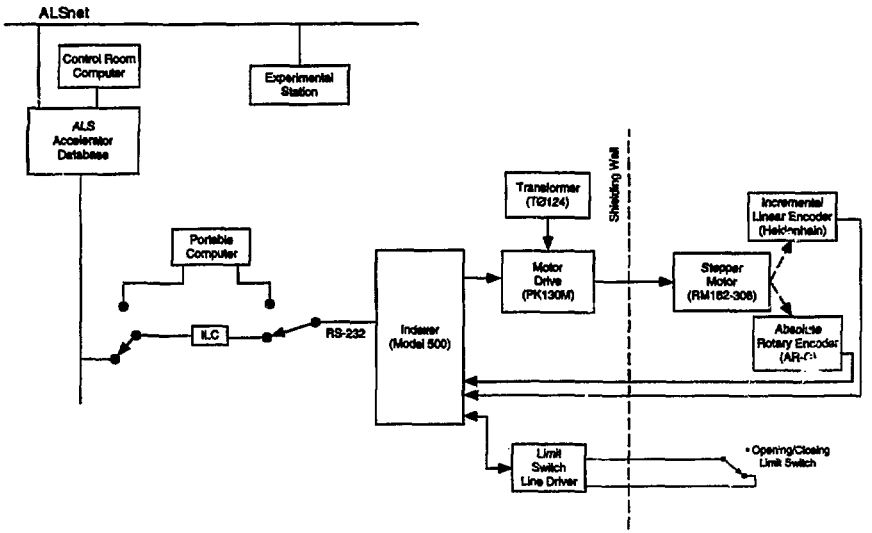

FIG. 29. Insertion device control system.

In order to accurately position the insertion device gap over the 210 mm range of motion, a considerable effort has been spent on the previous undulators in order to understand the drive system behavior. Using the absolute rotary encoder and a finely spaced calibration table, the achieved absolute accuracy of these systems is ± 5 μm. Although the motor drive system is capable of stepping in 0.0667 μm increments, due to the hysteresis and repeatability of the mechanical system, it is difficult to resolve steps less than a few microns. For a one micron step size moving unidirectional, one should expect a 0.2 μm error per step.

The only requirement that the previous insertion device motor control systems have difficulty obtaining is the positioning accuracy. In order to incrementally position the gap with a resolution below a few microns, the 10.0 Undulator will use a incremental linear encoder to directly read the gap position. A Heidenhain encoder has been selected. This system may still have difficulty in reaching an absolute positioning accuracy ± 1 μm, however three methods of "finding" the home position on power-up will be attempted. First, the absolute rotary encoder can provide, ± 5 μm absolute positioning at all times. Second, the repeatability of "hitting" the home reference mark on the incremental encoder will be determined. Third, by observing a known spectral line on the output of the monochromator, the gap could be accurately repositioned. Once the startup gap position is known, any incremental move from that point should be accurate to the sub-micron level.

The insertion device gap position can be easily controlled and monitored from the ALS control room or from the experimental stations via the ALSnet. The user has the options of setting the gap position [mm], gap velocity [mm/sec], and maximum rate of change of field strength [T/sec]. The gap velocity can also be profiled to any desired pattern which does not exceed the 2 Hz update rate on velocity change. The gap position is continuously monitored at approximately a 2 Hz update rate. As shown in Figure 29, one can bypass the main accelerator control system and establish local control at the ILC or directly at the Indexer by using a portable computer.

If required, compensation coils or end rotor systems can easily be retrofitted into the current control system design.

5.7 Vacuum System

The vacuum system for the U10.0 Undulator will be the U5.0 Undulator commissioning system with the windows widened.[29]

A plan view of the U10.0 undulator vacuum system is shown in Figure 30; the completed chamber is shown in Figure 31. The chamber has a 1.9 cm vertical aperture, and the thin pole windows will allow for a 2.335 cm minimum magnetic gap.

5.7.1 Vacuum Chamber

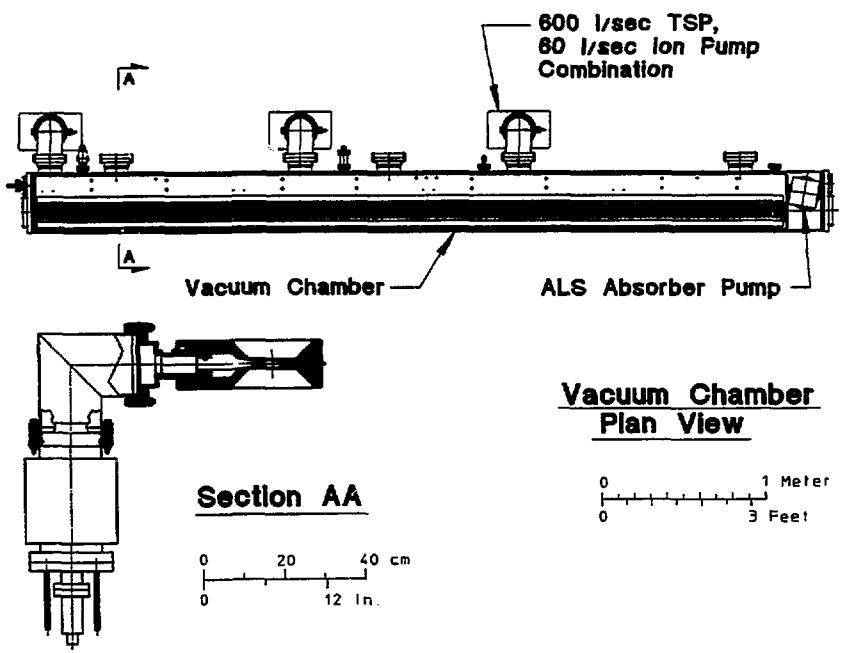

FIG. 30. Vacuum system layout.

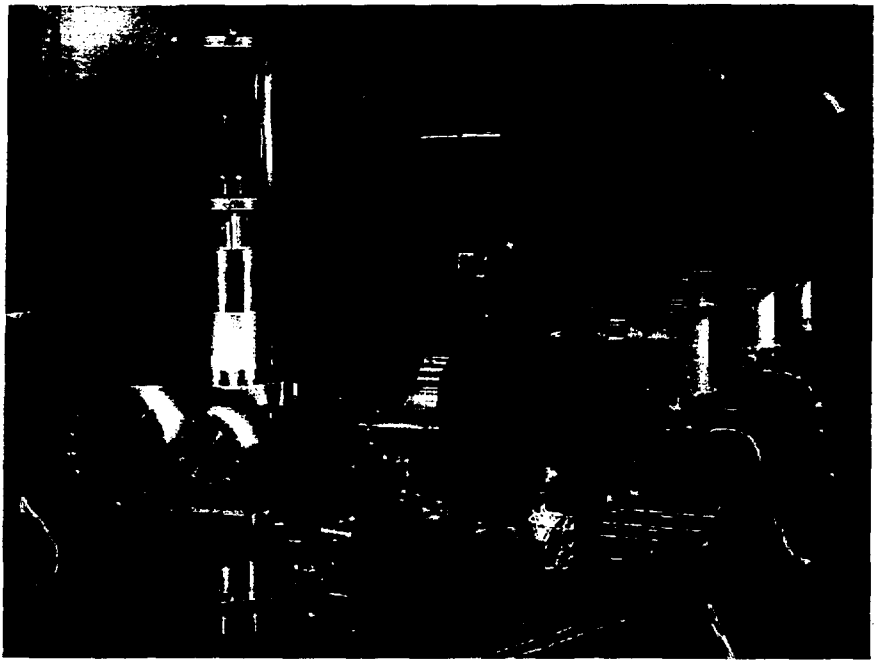

FIG. 31. Completed vacuum system.

The Insertion Device vacuum chamber, as shown in Figure 30, includes the vacuum chamber, six side ports and one top and bottom port near the exit end of the chamber for vacuum pumps as described in paragraph 5.7.2. Several smaller ports along the side of the chamber are used for a roughing system, ion gauge and an RGA head. There is also a flange located at the upstream end for insertion of a NEG pump. Figure 32 shows a cross sectional view of the chamber. The chamber 1.9 cm clear vertical aperture at the centerline with a profile that closely follows that of the storage ring sector chamber.

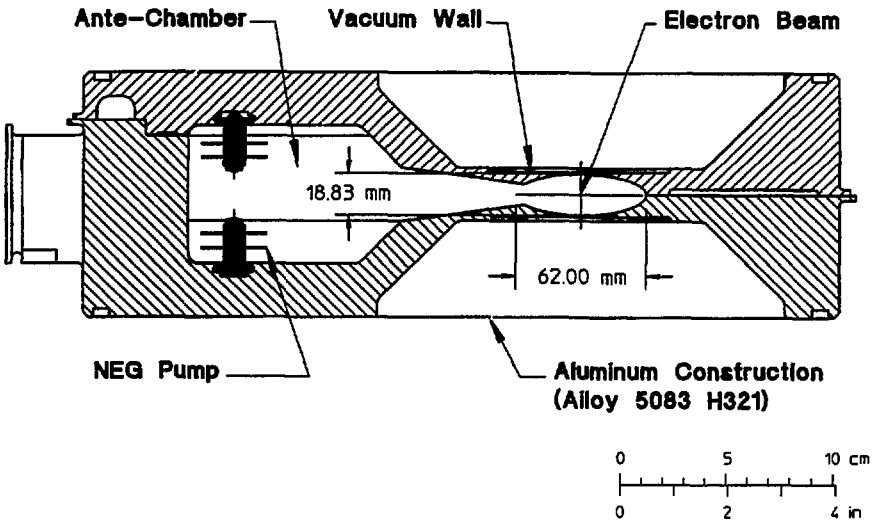

FIG. 32. Vacuum chamber cross-section.

The chamber is fabricated from aluminum alloy 5083 H321 plates. This material was chosen over stainless steel for economy and the fact that there is little difference in the radiation dosage to the CSEM material. The chamber is machined to provide a minimum horizontal gap of 21.8 cm, 3.2 cm to the inside circumference of the storage ring for the circulating beam aperture and 18.6 cm to the outside circumference to avoid bending magnet radiation from hitting the wall of the vacuum chamber. The chamber has an antechamber along the complete length and to the outside circumference for increased conductance for pumping. Most of the unwanted synchrotron radiation will be absorbed by the photon stop located at the exit end of the chamber. The outside of the chamber will have every other pocket machined into it widened for the magnet poles to achieve a minimum magnetic gap of 2.335 cm for operation.

Deflections and stresses were examined for the original vacuum chamber.[30] The critical area for the vacuum chamber is the area where the windows are only 0.75 mm thick and the adjacent wall thickness, which is only 2.75 mm. For the U10.0 chamber, the calculated deflection of the thin window alone is 8 mm.[31] The maximum stress in the adjacent wall thickness is less than 10,000 psi, which is acceptable because the design stress is 14,000 psi, 75% of the yield strength of 5083 H321 aluminum at 150 degree C, our bakeout temperature.

The following tolerance budget described in Table X shows how the minimum magnetic gap of 2.335 cm will be achieved with the vacuum chamber.

Table X. Vacuum chamber tolerance budget.

	mm
Clear aperture of the as-built chamber under vacuum	18.22
Window thickness 2 x 0.75 mm	1.50
Chamber flatness over 4.6 m	0.74
Installation tolerance (effect of pumps twisting chamber, and alignment)	0.69
Allowable interlock and hard stop allowance	0.86
Minimum IDB-U5.0 commissioning chamber magnetic gap under vacuum	22.62
Allowable U10.0 fabrication flatness, positional, and deflection tolerances	0.73
Minimum U10.0 Undulator minimum magnetic gap	23.35

Under normal operating conditions, the heat input to the insertion device vacuum chamber due to photons striking the top and bottom surfaces of the chamber from the last upstream gradient magnet is less than 10 watts.[32]

The effect of electron beam vertical missteering (during dedicated operation) was examined for the 1.0 cm high aperture vacuum chamber.[33] Allowing the chamber material to approach 80% of yield, due to thermal stresses, the maximum allowable vertical missteering angle is ± 0.6 mrad, which is acceptable since the projected beam would hit the wall of the sector vacuum chamber above—or below—the slot where the insertion device beam exits through the slot.

UHV preparation and bakeout of the chamber follows a specific procedure.[34] Bakeout is at 140 degrees Celsius for a minimum of 48 hours, and a base pressure of less than 3×10^{-10} Torr has been typically achieved after conditioning.

5.7.2 Pumping System Design

The vacuum pumping system proposed for the U10.0 vacuum chamber is shown in Figure 30. The pumping system consists of combination 600 l/s titanium sublimation and 60 l/s ion pumps of commercial manufacture, an ALS Absorber pump of 1450 l/s capacity, and 15 m of 3-cm-wide NEG (alloy ST707) pumping strips mounted above and below the midplane in the antechamber.

The combination pumps are located to provide an even pressure distribution throughout the chamber as well as missing support and drive system components. Each combination pump assembly consists of a transition piece from a rectangular port to a round port, a 90 degree elbow, and the pump. An ALS TSP Absorber pump is located at the exit end of the chamber. It consists of a photon stop that absorbs most of the unwanted synchrotron radiation directly over a TSP assembly and pumps the resulting gas load, which has been directed downward by the photon stop.

The ALS storage ring vacuum system is configured with seven sector valves that allow isolation of the injection straight, the RF straight, and splits the remaining ring into five sections. If necessary, seven more sector valves can be installed to allow each insertion device straight and adjacent down-stream arc sector to be isolated from the rest of the ring.

With this combination of pumps, calculations predict that the average pressure distribution should be less than 10^{-9} Torr in the vacuum chamber.[35, 36, & 37] Measurements taken on the U5.0 Undulator commissioning chambers, presently installed in the storage ring (January 1994), show a 1.4×10^{-10} Torr vacuum with 100 mA of circulating beam.

The nominal pumping speeds of the various pumps in the 5.0 m long antechamber are tabulated in Table XI.

Table XI. ALS commissioning vacuum chambers—pumping system.

Pump	Nominal pumping speed (l/s)
Combination 600 l/s tsp/60 l/s ion – 3 units	520
ALS absorber pump (tsp)	2400
NEG (Saes-type ST707/CTAM/30D strip–15 m)	4800

5.7.3 Insertion Device Vacuum Control and Diagnostics

There are three 60 l/s ion pumps with integral sublimation filaments on the system. The pumps are driven and monitored by ion pump controllers. These controllers are interfaced to the accelerator control system via the IEEE-488 bus. The titanium sublimation filaments are powered by a single power supply multiplexed to these three pumps. The frequency and duration of sublimation will be learned experimentally and controlled by an ILC.[38] It is expected that a few minutes sublimation once a week will be sufficient. Activation of the NEG strips is done with a 140 amp welder and a specific procedure is followed because chamber cooling is required so as not to partially demagnetize the magnetic structure.[39] Ion pumps and sublimation filaments on the sector arc chambers will be operated in the same fashion.

Monitoring of the ID vacuum chamber pressure is accomplished in two ways. The ion pump current is converted to approximate pressure in the local display. A voltage commensurate with ion pump current is supplied to the controlling ILC via the bus and is converted to pressure and presented to the operator as a pressure profile along the insertion device. Accurate pressure measurements in the UHV range are accomplished at one of two locations with nude ion gauges and an ion gauge controller. This controller measures pressure above a milliTorr with a thermocouple vacuum gauge. This allows pressure monitoring when the vacuum chamber is being roughed down. An ILC will control and monitor the ion gauge controller via the IEEE-488 bus. This monitoring technique is also used in the sector arc chambers.

5.7.4 Insertion Device Electron Beam Position Monitor (BPM)

Four button electrodes, similar in design to those in the sector arc chambers, will be installed in a symmetrical pattern about the beam centerline at each end of the ID, in the adjacent transition sections next to the flanges that connect to the ID vacuum chamber, to sense the electron beam. They are shown in LBL Drawing numbers 23L3456 and 23Q4406.

5.7.5 Vacuum Chamber and Pumping System Support

The vacuum chamber and pumping system is considered as one assembly for support purposes. Support of the assembly is from two six-inch-square, 15-feet-long beams mounted on the upper horizontal beams of the undulator support structure. The vacuum chamber is supported by four struts located near the quarter points, two on each side, and from two struts located at the center. After final installation, the chamber must be flat to within 0.1 mm. Additional supports are provided for the ion pump assemblies and the ALS TSP Absorber pump to not load the vacuum chamber. The support system is designed to electrically isolate the complete vacuum chamber assembly from the support and drive system and the magnetic structure.

5.8 Installation

Installation includes installation of the vacuum system into the undulator, preparatory tasks in preparation for the installation of the undulator and then the actual installation of the undulator into the storage ring.

A plan view of the undulator installed in the storage ring is shown in Figure 33. A tunnel view of an installed undulator is shown in Figure 26.

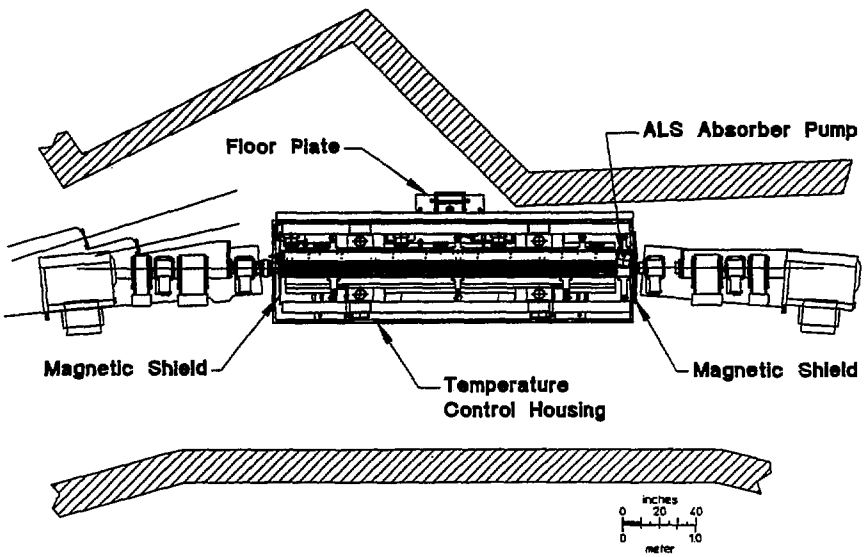

Fig. 33. Undulator installed in storage ring.

5.8.1 Vacuum chamber installation

Vacuum chamber installation is as follows:

1. Installation of the vacuum system support structure which includes installing the two large 5 m long support beams, the struts and associated connecting hardware.
2. Surveying and leveling the insertion device and then determining the vacuum chamber location by survey.
3. Installation of the vacuum chamber which has been back filled with dry nitrogen into the undulator with the installation fixture.
4. Installation of the pumping system, then pump down of the system and leak checking.
5. Vacuum system alignment and then the setting of the electrical and mechanical stops.

6. Lastly, installation of the magnetic shields and the temperature control housing around the undulator.

5.8.2 Installation Preparation

Tasks required prior to installation include:[40]

1. Surveying the locations of the floor mounting plates in the Storage Ring, core drilling the required holes, and installation of the Hilti anchor studs and floor mount base plates.

2. Surveying the floor mount base plate elevations, determining the kinematic floor mount shim plate thicknesses, fabrication of the shim plates and then installation of the kinematic floor mount shim plates.

3. Installation of cables from the insertion device control system rack to the insertion device in the Storage Ring.

5.8.3 Undulator installation into the Storage Ring

Installation requires the following tasks:

1. Remove the Storage Ring shielding in the appropriate straight section.

2. Vent the appropriate Storage Ring section, remove the straight section vacuum chamber, supports, stands and concrete pedestals.

3. Remove the magnetic shields and temperature control housing from the undulator.

4. Prepare the undulator for transport, unbolt the kinematic mounts(3), lift the undulator off the kinematic mounts, remove the kinematic mounts(3) and install the kinematic mounts(3) in the appropriate storage ring straight section.

5. Install the inside and outside temperature control housing frames in the Storage Ring.

6. Transport the undulator to the appropriate Storage Ring Section, install on the kinematic mounts and bolt down.

7. Remove the hoist equipment from the undulator and reinstall the Storage Ring shielding.

8. Survey in the undulator.

9. Take measurements for flex band installation and carry out the flex band installation.

10. Complete the remaining wiring and check out the system locally.[41]

11. Carry, out a UHV bakeout and activate the NEG and TSP pumps.[42]

12. Reinstall the temperature control housing frame and magnetic shields, clean the magnetic structure and vacuum system thin window areas, and install the temperature control housing panels.

13. Verify that the temperature interlock system operates correctly.

14. Checkout the drive system from the control room.[43, 44]

15. Place the undulator gap in the fully open position and place the undulator in administrative LOTO.[45]

References

[1] IDG-U10.0 Cost Estimate, (FY94).

[2] U8.0 Conceptual Design Report, LBL PUB-5276, (May 1990).

[3] B.M. Kincaid, Random Errors in Undulators and Their Effects on the Radiation Spectrum, SPIE Vol. 582, pp 72-83, (October 1985).

[4] K. Halbach, Insertion Device Design: 16 Lectures Presented from October 1988 to March 1989, LBL Publication V 8811-1.1-16.

[5] K. Halbach et al., Error Field Calculation in a Hybrid Insertion Device, (to be published).

[6] R. Schlueter, Engr. Notes, (1994).

[7] W. Hassenszahl, An Assessment of the Effects of Radiation on Permanent Magnet Material in the ALS Insertion Devices, LBL-27808.

[8] SLAC memo dated March 1, 1989, from Y. Namito, T. M. Jenkins, W. R. Nelson to W. V. Hassenzahl (LBL) summarizing EGS4 calculations of radiation doses on materials in insertion devices.

[9] U5.0 Undulator Conceptual Design Report, LBL PUB-5256, (November 1989).

[10] E. Hoyer, Periodic Structure Magnetic Design, LBL Engr. Note M7412A, (December 1993).

[11] K. Halbach, et al., developed PANDIRA, and improved version of POISSON, which allows solution of permanent magnet and residual field problems; POISSON is an improved version of TRIM [A. M. Winslow, J. Computer Phys. 1, 149, (1967)].

[12] D. Humphries, INSORT, A Sorting Code for Hybrid Permanent Magnet Structures, LBL Engr. Note M7427, (September 1993).

[13] W. Press, et al., Numerical Recipes—The Art of Scientific Computing, Cambridge: Cambridge University Press, pp. 326–334, 1986.

[14] E. Hoyer, Multiple Trim Magnets, LBL Engr. Note M7354, (May 1993).

[15] E. Hoyer, Magnetized Neodymium-Iron-Boron Blocks, LBL Specification M793, (June 1993).

[16] E. Hoyer, Flux Shunt Magnetic Measurements on IDB, Engr. Note M7350, (April 1993).

[17] E. Hoyer, Backing Beam Design Calculations, LBL Engr. Note, M6834, (May 1989).

[18] D. Humphries, et al., Precision Alignment of the Advanced Light Source U5.0 and U8.0 Undulators, Proceedings of the SPIE 1993 International Symposium on Optical Applied Science and Engineering, San Diego, California, July 11–16, 1993, LBL-33237.

[19] E. Hoyer, Magnetic Nd-Fe-B Block Measurement Procedure, LBL Engr. Note M7058, (September 1990).

[20] S. Marks, Helmholtz Coil Block Measurement Facility—Operational Procedure, LBL Engr. Note M7102, (January 1991).

[21] S. Marks, et al., Insertion Device Magnet Measurements for the Advanced Light Source, 1993 IEEE-PAC Conference, May 1993, LBL-33229.

[22] J. Chin, Site Elevation and Floor Shim Adjustment, LBL Engr. Note M7259, (October 1993).

[23] J. Chin, U8.0 Magnetic Load Compensating Spring, LBL Engr. Note M7228, (September 1993).

[24] J. Chin, Drive System Backlash, LBL Engr. Note M6882, (August 1989).

[25] G. Portman, IDB test result to be published.

[26] J. Chin, Assembly and Alignment Notes, LBL Engr. Note M7349, (September 1993).

[27] J. Chin and W. Gath, Backing Beam Assembly and Alignment Notes, LBL Engr. Note M7435, (October 1993).

[29] J. Chin, *Support and Drive System Production/Inspection Record form.*

[29] D. Plate, IDA/IDB–U5.0 Vacuum System Fabrication Record (PIR) for Vacuum Chambers, LBL Engr. Note M7292, (August 1992).

[30] E. Hoyer, Vacuum Chamber Design, LBL Engr. Note, M6806, (February 1989).

[31] E. Hoyer, U5.0 Commissioning Vacuum Chamber—Changes for U10.0, LBL Engr. Note M7458, (July 1993).

[32] E. Hoyer, Photon Heating of the Undulator Vacuum Chamber, LBL Engr. Note, M6877, (July 1989).

[33] E. Hoyer, Maximum Permissible Vertical Missteering Angle, LBL Engr. Note, M6833, (May 1989).

[34] D. Plate and W. Gath, Insertion Device Vacuum Chamber Bakeout Procedure, LBL Engr. Note M7304, (September 1992).

[35] E. Hoyer, Pumping System Design Calculations, LBL Engr. Note M6821, (March 1989).

[36] E. Hoyer, CDR Vacuum Chamber Pressure Distribution, LBL Engr. Note M6844, (May 1989).

[37] E. Hoyer, Chamber Pressure Improvement with NEG Pumping, LBL Engr. Note, M6889, (September 1989).

[38] D. Plate and W. Gath, Activation of NEG (Non-Evaporable Getter) for All ALS Insertion Device Vacuum Systems, ALS Procedure ID-02-04, (January 1994).

[39] E. Hoyer, NEG Power Requirements and Chamber Cooling, Engr. Note M7273, (April 1992).

[40] J. Chin , E. Hoyer, Installation and Removal of ALS Insertion Devices — IDA, IDB Undulators, ALS Procedure ID 02-02, (October 1993).

[41] K. Gershon, G. Portmann, Operating the Installed Insertion Device Motor Control Locally, ALS Procedure ID 02-05, (January 1994).

[42] D. Plate, Undulator Bakeout, ALS Procedure ID 02-03, (March 1994).

[43] J. Young, *Testing of Instrument Control Software*, ALS Procedure CS 02-0_, (October 1993).

[44] G. Portmann, Operating the Insertion Device Gap Motor Control System from the Control Room, ALS Procedure CS 02-03, (October 1993).

[45] J. Chin, E. Hoyer, Undulators IDA, IDB, and IDC Lockout/Tagout (LOTO) Procedure, ALS Procedure ID 09-01, (October 1993).